J. Mech. Phys. Solids 174 (2023) 105259

Contents lists available at ScienceDirect

Journal of the Mechanics and Physics of Solids

journal homepage: www.elsevier.com/locate/jmps

# A chemo-mechanical coupling model of oxidation and interlayer cracking of copper nanowires

Yulong Gong [a,b], Xin Yan [c], Jici Wen [d], Qinghua Meng [a], Ang Li [e], Xinghua Shi [a,b,*]

[a] Laboratory of Theoretical and Computational Nanoscience, CAS Center for Excellence in Nanoscience, National Center for Nanoscience and Technology, Chinese Academy of Sciences, Beijing 100190, China
[b] University of Chinese Academy of Sciences, No. 19A Yuquan Road, Beijing 100049, China
[c] School of Mechanical Engineering and Automation, Beihang University, Beijing 100091, China
[d] State Key Laboratory of Nonlinear Mechanics (LNM), Institute of Mechanics, Chinese Academy of Sciences, Beijing 100190, China
[e] Beijing Key Lab of Microstructure and Properties of Advanced Materials, Beijing University of Technology, Beijing 100124, China

ARTICLE INFO

*Keywords:*
Chemo-mechanical coupling
Interlayer cracking
ReaxFF
Energy release rate
Oxidation
Copper nanowires

ABSTRACT

Copper nanowires have received extensive attention for their potential applications in optics, electricity and catalysis, while oxidation erosion has become the biggest obstacle to their widespread application. Here, we present a chemo-mechanical coupling model to investigate the interlayer cracking behaviors of nanowires during oxidation. In contrast to existing chemo-mechanical models, the present model emphasizes that the process of oxygen entry into copper nanowires is chemical reaction-mediated layer-by-layer replacement rather than vacancy-mediated diffusion, which means the oxygen ions in the outer layer would not cross over the oxygen atoms in the inner layer during their entry. These conclusions are validated by molecular dynamics simulations. We then discuss the effect of the chemical reaction-induced free energy on the stress state of the nanowire during the reaction. Finally, a self-developed finite difference procedure is used to solve the control equations and the fracture location is determined according to the energy release rate analysis. We find the fracture of nanowires is closely dependent on the size of nanowire, the reaction rate and the oxygen concentration. This work deepens our understanding of the mechanism of chemo-mechanical coupling and fracture behavior of metals due to oxidation, thus has implications in other areas involving chemo-mechanical coupling.

## 1. Introduction

Copper, one of the first metals used by humans, is still widely used in various areas of our daily life such as construction materials, electrical systems and electronic devices (Gattinoni et al., 2015). The properties of copper have been extensively studied in recent decades, while the oxidation and corrosion of this metal have not been fully solved, which severely influences its performance in industrial and technological applications. Since copper has been found to oxidize at room temperature (Iijima et al., 2006; Platzman et al., 2008), there is an urgent desire to find ways to prevent copper oxidation, making it promising as an environmentally friendly, low-cost alternative in tin-lead or gold/silver-based solder alloys in electronic packaging (Song et al., 2012). For example, the voids due to copper oxidation in the connections of many nano-electronic devices and nano-electromechanical systems are not desired (Huang et al., 2018). Then it is necessary to first study the oxidation and corrosion of copper under oxygen-rich conditions. Not all

* Corresponding author.
*E-mail address:* shixh@nanoctr.cn (X. Shi).

https://doi.org/10.1016/j.jmps.2023.105259
Received 21 December 2022; Received in revised form 9 February 2023; Accepted 28 February 2023
Available online 5 March 2023

**Table 1**
Representative material parameters for the nanowire.

| Parameters | Symbols | Values | Units |
|---|---|---|---|
| Young's modulus of pure copper | $E_0$ | 74 | GPa (Hui et al., 2020) |
| Poisson's ratio | $\nu$ | 0.34 | - |
| | $m$ | 0.45 | - (Sondors et al., 2020) |
| Chemical modulus | $\zeta$ | - | kJ/mol |
| $\zeta^* = \zeta/(RT)$ | $\zeta^*$ | 0, 3 or 6 | - |
| Partial molar volume | $\Omega$ | 0.74 | - (Su et al., 2014) |
| Diffusion coefficient of O in Cu | $D_0$ | - | $m^2/s$ |
| | $\alpha$ | 0.95 | - |
| Radius of the nanowire | $b$ | 20 | nm |
| Time | $t$ | - | s |
| $t^* = D_0 t/b^2$ | $t^*$ | 0.005 or 0.01 | - |

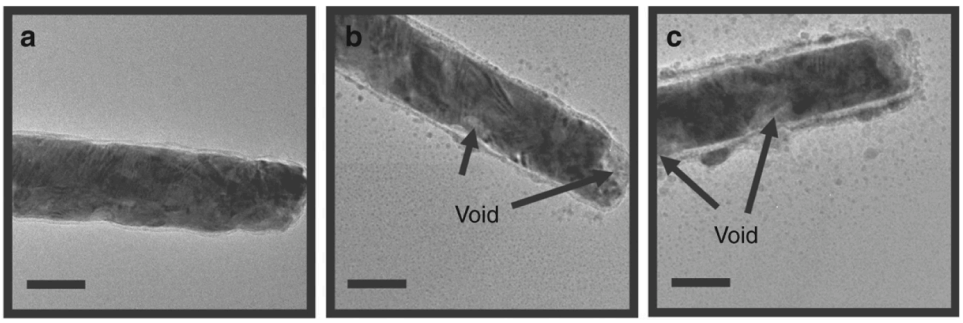


**Fig. 1.** Bright-field TEM images of the copper nanowire (CuNWs). a-c Nanocrystalline CuNW after air-exposure for less than 1 day (a), 3 days (b) and 7 days (c) (Huang et al., 2018).

oxidation is undesirable. In recent years, hollow or core-shell nanostructures have been synthesized by oxidation reaction of nanowires with remarkable results in the fields of fuel cells, drug delivery, catalysts, biosensors and plasmas (Liu et al., 2014; Caruso et al., 1998; Kim et al., 2002; Xie et al 2011; Oldendurg et al., 1998). Understanding the mechanism of formation of layer cracking behavior during the oxidation of nanowires is fundamental in terms of exploiting the layer cracking process to obtain hollow nanotubes, core-shell structures.

Table 1

The oxidation process in coppers typically involves 3 processes: (1) the chemical reaction between oxygen and copper atoms; (2) the diffusion of oxygen ions driven by a concentration gradient; (3) the volume expansion of coppers due to the embedding of oxygen ions. The oxidation reaction is inevitably accompanied by the breaking/reforming chemical bonds between the oxygen and copper atoms. The released reaction energy and the concentration gradient of oxygen within the coppers drive the diffusion of oxygen ions inward, facilitating the oxidation reaction forward. As the driving force is balanced by the accumulated internal stress induced by the embedding of oxygen ions, the diffusion of oxygen ions ceases at some position, resulting in a nonuniform distribution within the coppers. Further oxidation may accumulate high internal strain energy, leading to layer crack of coppers. For instance, Huang et al. (2018) have experimentally observed that after exposure of copper nanowire to air for several days, the oxide layer gradually thickens until the interlayer fractures (Fig. 1).

This chemo-mechanical coupling process is very similar to the charging and discharging process of high-capacity lithium batteries. The oxidation behavior of copper and the charging behavior of Li-ion batteries have exactly the same mechanical process, *i.e.*, the volume expansion of coppers/silicon electrodes due to the embedding of oxygen/Li ions. However, Studies have shown that Li diffusion in Si involves vacancy mediation (Moon et al., 2016). So most studies of Li batteries are based on the coupling of diffusion of Li ions and elastic and plastic deformation of the electrode (Christensen and Newman, 2006; Zhang et al., 2007; Cheng and Verbrugge, 2009; Golmon et al., 2010; DeLuca et al.,2011; Ryu et al., 2011; Grantab and Shenoy, 2012; Haftbaradaran et al., 2010, 2011; Gao and Zhou, 2011). Although there have been some reports on the mechanism of copper oxidation (Byoungseon et al., 2011), the effect of chemical reaction on oxygen diffusion remains unclear. Moreover, there is a lack of accurate theoretical model to describe the change in stress and failure behavior during the oxidation of copper. Therefore, it is necessary to investigate the effect of chemical reactions (charge transfer) on oxygen diffusion in copper from the atomic scale and to develop a new mechanical-chemical coupling model to study the stress and interlayer cracking behavior of nanowires.

In this paper, we use a copper nanowire as a model system to study its oxidation and fracture behavior. In Section 2, we first propose a chemo-mechanical coupling model in which the reaction and diffusion driven by oxygen concentration gradients are considered. A self-developed finite difference method is then used to solve the model. In Section 3, we further study the initiation of crack during the spallation of copper nanowires. The energy release rate is calculated and used as a criterion to determine the fracture location. In Section 4, we conduct molecular dynamics simulations with reaxFF force field to study the oxidation process of coppers, and examine

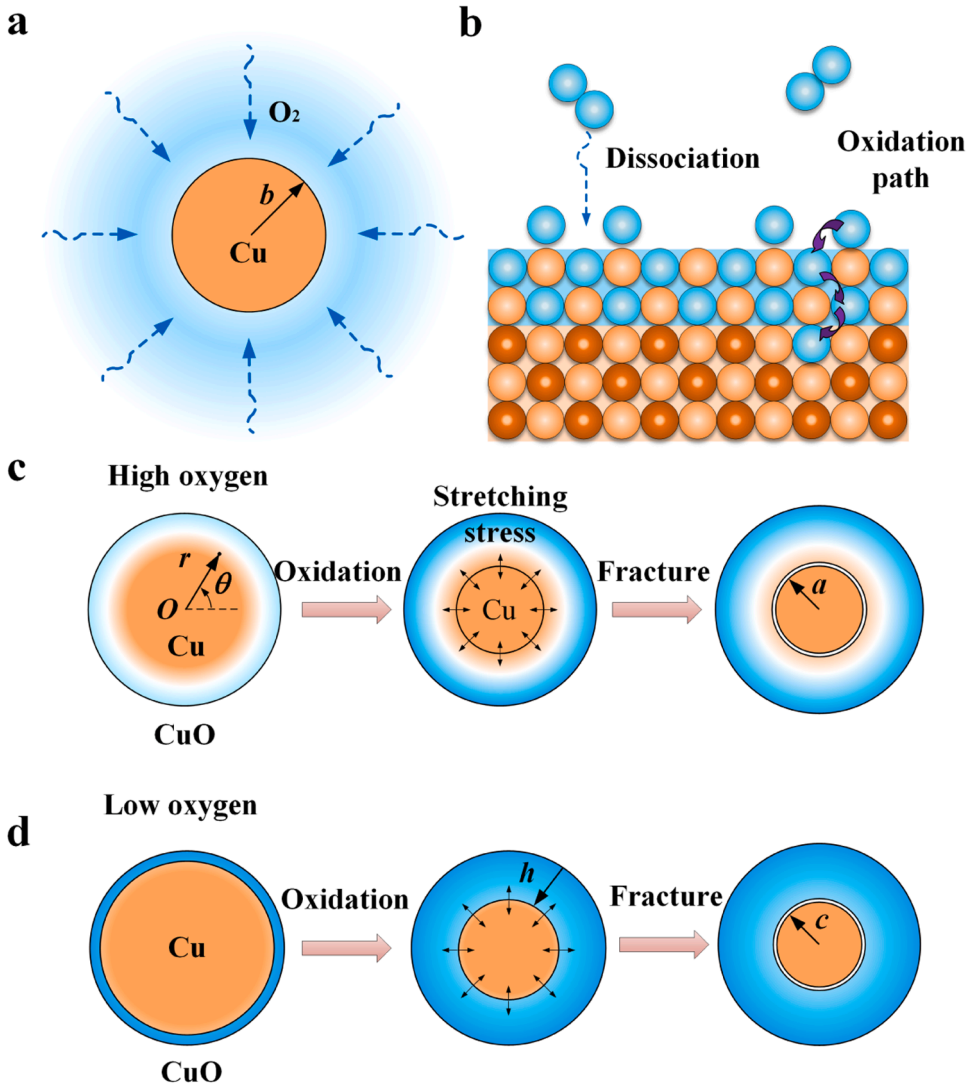


**Fig. 2.** (a) Schematic cross-section of the copper nanowire before oxidation. (b) Schematic of the copper nanowire oxidation process. (c) Schematic of the oxidation process and interlayer cracking behavior of the copper nanowire under high oxygen conditions. (d) Schematic of the oxidation process and interlayer cracking behavior of the copper nanowire under low oxygen conditions.

the effect of charge transfer on the diffusion pathway of oxygen ions. The effects of chemical reactions on the concentration and stress fields of oxygen during the oxidation are then discussed. Finally, a summary is provided in Section 5.

## 2. Mechanical-chemical coupling model

During the oxidation, once an oxygen molecule in the external environment toughs the copper surface, it dissociates into two oxygen atoms which further react with the copper atoms to become oxygen ions. The chemical reaction between oxygen and copper atoms consists of two steps. First, oxygen molecules are dissociated into oxygen ions, reacting with copper atoms to form copper oxide or cuprous oxide, *i.e.*,

$$O_2 + 4e^- \rightarrow 2O^{2-},\ Cu \rightarrow Cu^{k+} + ke^-,$$

$$2/kCu^{k+} + O^{2-} \rightarrow Cu_{2/k}O.\ (k=1 \text{ or } 2)$$

Then, the chemical potential gradient resulting from the uneven distribution of oxygen ions in the nanowire drives these oxygen ions toward the center of nanowire, reacting with neighboring copper atoms inside. Obviously, the chemical reaction is accompanied by the diffusion of oxygen ions, resulting in the gradual oxidation of nanowire from surface to center. The absence or presence of a finite interface between copper and copper oxide is used as a criterion for defining low or high concentrations, which significantly

affect the oxidation behavior of copper nanowires (Prisedsky and Vinogradov, 2004). When copper nanowire is exposed to a sufficient amount of oxygen atmosphere, relative fast diffusion of oxygen ions leads to partial oxidation, resulting a transition region between the copper and copper oxide regions, as shown in Fig. 2c. When the oxygen in the environment is not sufficient, slow diffusion of oxygen ions leads to full oxidation, resulting a distinct interface formed between copper oxide and pure copper regions (Zhou et al., 2012), as shown in Fig. 2d. Here we develop the models under high and low oxygen concentration conditions, respectively. To simplify the problem, we assume the degree of oxidation along the axial and circumferential directions of the nanowire is the same. Then it becomes a 2-dimensional problem. The formation of copper oxide leads to a volume expansion, inducing tensile stress along the radial direction in the nanowire. As the oxidation reaction advances, the strain energy of nanowire gradually accumulates and approaches a critical value. Then the interlayer cracking occurs at certain location to release the strain energy, dividing the nanowire into two parts: a small copper nanowire and a hollow nanotube as shown experimentally (Huang et al., 2018).

Herein we will develop a theoretical model to describe the chemo-mechanical coupling behavior of copper nanowire during oxidation.

### 2.1. Interlayer cracking of nanowire under high oxygen concentration

As previously mentioned, the oxidation of copper nanowires involves three components, *i.e.*, diffusion of oxygen ions, chemical reaction between oxygen and copper atoms and volume expansion of nanowire. The free energy of the system can be expressed as the sum of energies of three components, *i.e.*,

$$U = U_{\mathrm{d}} + U_{\mathrm{r}} + U_{\mathrm{e}}, \tag{1}$$

where $U_{\mathrm{d}}$, $U_{\mathrm{r}}$ and $U_{\mathrm{e}}$ are the chemical energy of oxygen diffusion, the chemical reaction energy and elastic strain energy induced by volume expansion, respectively. Under high oxygen condition, the oxygen ions diffuse towards the center of the nanowire under enormous gradient of chemical potential. The diffusion of oxygen ions into copper nanowires is inevitably accompanied by oxidation reactions of oxygen and copper atoms. Meanwhile the interaction between oxygen and copper atoms also affects the diffusion of oxygen ions in the copper nanowire.

Let $\phi$ denote the concentration of oxygen ions in the copper oxides, in which $\phi = 0$ and 1 refer to the cases of pure copper and pure copper oxide, respectively. The diffusion behavior of oxygen ions is only related to their concentration gradient. Following the work of Wei et al. (2010), the chemical energy associated with the diffusion can be expressed as

$$U_{\mathrm{d}} = \mu^0\phi + RT\phi(\ln\phi - 1), \tag{2}$$

where $\mu^0$ is the reference chemical potential, $R$ is the gas constant and $T$ is the absolute temperature. The effect of charge transfer, *i.e.*, chemical reaction, on the chemical process of oxygen ions is studied via molecular dynamics simulations in Section 4, which has been found to promote the entry of oxygen ions into the nanowire. The chemical reaction energy between the oxygen and copper atoms (Loeffel and Anand, 2011) is described as

$$U_{\mathrm{r}} = \frac{1}{2}\zeta(1-\phi)^2, \tag{3}$$

where $\zeta$ is the chemical modulus related to the reaction temperature. After the embedding of oxygen ions, a volume expansion generates stress in nanowire. In this process, the deformation of nanowire is associated with the movement of copper atoms. We consider the copper nanowire and copper atoms as a continuum solid and material points, respectively. Then the elastic strain energy of the nanowire (Gao and Hong, 2016) can be written as

$$U_{\mathrm{e}} = \frac{\lambda}{2}(E_{kk})^2 + \nu E_{ij}E_{ij}, \tag{4}$$

where $\lambda$ and $\mu$ are the Lamé constants, $\boldsymbol{E}$ is the Green-Lagrange strain tensor. By substituting Eqs. (2), (3) and (4) into Eq. (1), the free energy of the nanowire system can be written as

$$U = \mu^0\phi + RT\phi(\ln\phi - 1) + \frac{1}{2}\zeta(1-\phi)^2 + \frac{\lambda}{2}(E_{kk})^2 + \nu E_{ij}E_{ij}. \tag{5}$$

After quantifying the free energy of the system, we analyze the stress distribution in the oxidized nanowire resulting from the volume expansion. Based on the geometry of nanowire, a cylindrical coordinate system ($r$, $\theta$, $z$) is used to describe its deformation state, as shown in Fig. 2. The radius of nanowires is denoted as $b$. Due to a long cylinder of the nanowire, its stress state satisfies the plane strain condition, *i.e.*,

$$\varepsilon_z = 0, \tag{6}$$

where $\varepsilon_z$ is the strain in the axial direction of nanowire. The radial strain $\varepsilon_r$, circumferential strain $\varepsilon_\theta$ and axial strain $\varepsilon_z$ are

$$\varepsilon_r = \frac{\partial u_r}{\partial r},\ \varepsilon_\theta = \frac{u_r}{r},\ \varepsilon_z = \frac{\partial w}{\partial r}, \tag{7}$$

where $u_r$ and $w$ is the radial and axial displacements. When oxygen ions enter into the copper nanowire, its lattice size increases with the concentration of oxygen, giving rise to a variation of stress and strain states. By analogy with thermoelastic equations, the constitutive equations of oxidized nanowire are expressed as (Zhang et al., 2007)

$$\begin{aligned}
\varepsilon_r - \frac{\Omega}{3}\phi &= \frac{1}{E}[\sigma_r - \nu(\sigma_\theta + \sigma_z)],\\
\varepsilon_\theta - \frac{\Omega}{3}\phi &= \frac{1}{E}[\sigma_\theta - \nu(\sigma_r + \sigma_z)],\\
\varepsilon_z - \frac{\Omega}{3}\phi &= \frac{1}{E}[\sigma_z - \nu(\sigma_r + \sigma_\theta)],
\end{aligned} \tag{8}$$

where $\sigma_r$, $\sigma_\theta$ and $\sigma_z$ are the radial, circumferential and axial stresses, respectively, and $\nu$ and $\Omega$ denote the Poisson's ratio and partial molar volume of oxidized nanowire, respectively. The Young's modulus $E$ is written as (Shenoy et al., 2010)

$$E = E_0(1 + \phi m), \tag{9}$$

where $E_0$ is the Young's modulus of the nanowire before oxidation and $m$ is a dimensionless factor. The stress state of the nanowire during the oxidation is in a static equilibrium. According to elastic mechanics, the equilibrium equation is

$$\frac{\mathrm{d}\sigma_r}{\mathrm{d}r} + \frac{\sigma_r - \sigma_\theta}{r} = 0. \tag{10}$$

Furthermore, both the radial displacement in the center of nanowire and the radial stress on the surface are zero. Therefore, the boundary conditions are

$$u_r|_{r=0} = 0,\ \sigma_r|_{r=b} = 0. \tag{11}$$

By considering the conditions of Eq. (11) and substituting Eqs. (7)-(8) into Eq. (10), we have

$$\begin{aligned}
\sigma_r &= \frac{\Omega E}{3(1-\upsilon)}\left(\frac{1}{b^2}\int_0^b \phi r\mathrm{d}r - \frac{1}{r^2}\int_0^r \phi r\mathrm{d}r\right),\\
\sigma_\theta &= \frac{\Omega E}{3(1-\upsilon)}\left(\frac{1}{b^2}\int_0^b \phi r\mathrm{d}r + \frac{1}{r^2}\int_0^r \phi r\mathrm{d}r - \phi\right),\\
\sigma_z &= \frac{\Omega E}{3(1-\upsilon)}\left(\frac{2}{b^2}\int_0^b \phi r\mathrm{d}r - \phi\right).
\end{aligned} \tag{12}$$

It can be seen from Eq. (12) that the stress distributions of the nanowire are associated with the concentration of oxygen ions during the oxidation process.

We now establish a governing equation to describe the evolution of the oxygen concentration with respect to the oxidation time. Based on the law of conservation of mass, the diffusion equation of oxygen ions in the copper nanowire along the radial direction can be expressed as (Carslaw and Jaeger, 1959)

$$\frac{\partial \phi}{\partial t} + \nabla \cdot J = 0, \tag{13}$$

where $\nabla\cdot$ is the divergence and $J$ is the diffusion flux that represents the mass of oxygen ions flowing through unit area per unit time. Furthermore, the diffusion flux $J$ can be described as a function of the gradient of the chemical potential (Zhang et al., 2007)

$$J = -\frac{D\phi}{RT}\frac{\partial \mu}{\partial r}, \tag{14}$$

where the diffusion coefficient $D$ of oxygen ions in the oxidized nanowire (Yang et al., 2014) is written as

$$D = D_0\left(\frac{1}{1-\alpha\phi}\right), \tag{15}$$

where $D_0$ is the diffusion coefficient of oxygen ions in pure copper and $\alpha$ denotes a positive dimensionless coefficient. The chemical potential of oxygen ions $\mu$ is the partial derivative of the free energy $U$ of the system (Anand, 2012), *i.e*,

$$\mu = \frac{\partial U}{\partial \phi}. \tag{16}$$

By substituting Eq. (5) into Eq. (16), $\mu$ is written as

$$\mu = \mu^0 + RT\ln\phi + \zeta(\phi - 1) - \sigma_{\mathrm{m}}\Omega. \tag{17}$$

By substituting Eq. (12) into $\sigma_{\mathrm{m}}$, the hydrostatic pressure is

$$\sigma_{\mathrm{m}} = \frac{1}{3}(\sigma_r + \sigma_\theta + \sigma_z) = \frac{2\Omega E}{9(1-\nu)}\left(\frac{2}{b^2}\int_0^b \phi(r) r \mathrm{d}r - \phi(r)\right). \tag{18}$$

By substituting Eqs. (17) and (18) into Eq. (14), the diffusion flux along the radial direction $J$ can be expressed as

$$J = -D_0\left(\frac{1}{1-\alpha\phi}\right)\left[\frac{\partial\phi}{\partial r} + \frac{1}{RT}\left(\zeta + \frac{2E\Omega^2}{9(1-\nu)}\right)\phi\frac{\partial\phi}{\partial r}\right]. \tag{19}$$

Substituting Eq. (19) into Eq. (13), we have

$$\begin{aligned}\frac{\partial\phi}{\partial t} = D\Bigg\{&\frac{\partial^2\phi}{\partial r^2} + \frac{1}{r}\frac{\partial\phi}{\partial r} + \frac{\zeta}{RT}\left[\frac{\phi}{r}\frac{\partial\phi}{\partial r} + \left(\frac{\partial\phi}{\partial r}\right)^2 + \phi\frac{\partial^2\phi}{\partial r^2}\right] + H\phi\frac{\partial E}{\partial r}\frac{\partial\phi}{\partial r} + HE\left(\frac{\partial\phi}{\partial r}\right)^2 \\ &+H\phi\left(\frac{\partial^2 E}{\partial r^2}\phi + 2\frac{\partial E}{\partial r}\frac{\partial\phi}{\partial r} + E\frac{\partial^2\phi}{\partial r^2} + \frac{1}{r}\frac{\partial E}{\partial r}\phi + \frac{E}{r}\frac{\partial\phi}{\partial r}\right)\Bigg\} \\ &-\frac{\partial D}{\partial r}\left[\frac{\partial\phi}{\partial r} + \left(\frac{\zeta}{D} + H\right)\cdot\phi\frac{\partial\phi}{\partial r}\right],\end{aligned} \tag{20}$$

where the parameter $H$ is $H = \frac{2\Omega}{9(1-\nu)RT}$. Furthermore, the oxidation reaction of nanowire is carried out in an oxygen-rich environment. The concentration of oxygen $\phi$ on the surface of nanowire is considered as 1 while the initial concentration of oxygen in the nanowire is 0. In the entire reaction process, the concentration of oxygen at the center of nanowire has a finite value. Therefore, the boundary conditions of oxygen concentration are

$$\phi(b,t) = 1,\ \phi(r,0) = 0,\ \frac{\partial\phi}{\partial r}(0,t) = 0. \tag{21}$$

Since it is difficult to find an explicit expression of Eq. (20), the concentration of oxygen $\phi$ in the nanowire will be calculated by numerical method. Furthermore, the stress distribution in the nanowire can be obtained by substituting the resulting $\phi$ value into Eq. (12).

As the oxidation reaction advances, the elastic strain energy of the nanowire gradually accumulates. Based on classical Griffith's fracture theory, when the energy release rate of copper oxide $G$ reaches a critical value, the interlayer cracking within the nanowire occurs (Zhao et al., 2010). Here based on results of molecular dynamics simulations (see details in Appendix B), we find that the fracture toughness of the interface of Cu/CuO is much lower than that of copper oxide, thus the fracture is presumed to be occurred in the interface of Cu/CuO. In this way, the nanowire divides into two parts with new surface created: an inner copper nanowire and an outer hollow nanotube of oxidized copper. As such, the energy release rate $G$ is the difference in the strain energies, $U_{\mathrm{e}}$ and $U_{\mathrm{e}}'$, of the system before and after interlayer cracking divided by the area of the surfaces, *i.e.*,

$$G = \frac{U_{\mathrm{e}} - U_e^{'}}{2\pi a}, \tag{22}$$

where $a$ is the inner radius of the hollow nanotube. The strain energy $U_{\mathrm{e}}$ can be written as

$$U_{\mathrm{e}} = 2\pi\int_0^b e(r) r \mathrm{d}r, \tag{23}$$

where $e(r)$ is the strain energy density of the oxidized nanowire, which is expressed as

$$e(r) = \frac{1}{2E}\left(\sigma_r^2 + \sigma_\theta^2 + \sigma_z^2\right) - \frac{\nu}{E}\left(\sigma_r\sigma_\theta + \sigma_\theta\sigma_z + \sigma_z\sigma_r\right). \tag{24}$$

The strain energy $U_{\mathrm{e}}'$ equals to the sum of strain energies of smaller nanowire and hollow nanotube, *i.e.*,

$$U_{\mathrm{e}}^{'} = 2\pi\int_0^a e_i(r) r \mathrm{d}r + 2\pi\int_a^b e_o(r) r \mathrm{d}r, \tag{25}$$

where $e_{\mathrm{i}}$ and $e_{\mathrm{o}}$ are the strain energy densities of copper nanowire and hollow nanotube, respectively, which can be written as

$$e_i(r) = \frac{1}{2E}\left[\left(\sigma_r^i\right)^2 + \left(\sigma_\theta^i\right)^2 + \left(\sigma_z^i\right)^2\right] - \frac{\nu}{E}\left(\sigma_r^i\sigma_\theta^i + \sigma_\theta^i\sigma_z^i + \sigma_z^i\sigma_r^i\right), \tag{26}$$

$$e_o(r) = \frac{1}{2E}\left[\left(\sigma_r^o\right)^2 + \left(\sigma_\theta^o\right)^2 + \left(\sigma_z^o\right)^2\right] - \frac{\nu}{E}\left(\sigma_r^o\sigma_\theta^o + \sigma_\theta^o\sigma_z^o + \sigma_z^o\sigma_r^o\right), \tag{27}$$

where $\sigma_r^i$, $\sigma_\theta^i$ and $\sigma_z^i$ are the radial, circumferential and axial stresses of copper nanowire, respectively, and $\sigma_r^o$, $\sigma_\theta^o$ and $\sigma_z^o$ are the radial, circumferential and axial stresses of hollow nanotube, respectively.

The stress states in nanowire and hollow nanotube after interlayer cracking, and the details of the full expression for the energy release rate $G$ are listed in Appendix A.

### 2.2. Interlayer cracking of nanowire under low oxygen concentration

Under low oxygen and high temperature condition, the copper nanowire is oxidized layer-by-layer from outside to inside, as shown in Fig. 2d. In this process, the interface between copper oxide and copper regions in the nanowire moves gradually from surface to center. The cracking at the interface occurs when the strain energy release rate of the interface reaches the threshold value. We assume that the concentration of oxygen $\phi$ in the copper region equals to zero while $\phi$ is 1 in the copper oxide region.

For simplicity, the moving rate of the interface in the nanowire is considered as a constant $\eta$. The variation of the thickness $h$ of the copper oxide region with time $t$ can be expressed as

$$\frac{\mathrm{d}h}{\mathrm{d}t} = \eta. \tag{28}$$

Since the initial thickness of copper oxide is zero, by solving Eq. (32) $\eta$ can be expressed as

$$h = \eta t. \tag{29}$$

In this case, both the deformation and stress states in the copper and copper oxide regions still satisfy the forms of Eqs. (7), (8) and (10). Based on the above assumption, both the radial displacement in the center of nanowire and the radial stress on the surface equal to zero. The radial displacement at the interface between the copper region and copper oxide region should be continuous. Hence, the boundary conditions are

$$u_r^{\alpha}(0) = 0,\ u_r^{\alpha}(c) = u_r^{\beta}(c),\ \sigma_r^{\beta}(b) = 0, \tag{30}$$

where $c$ is the radius of copper region, the superscripts $\alpha$ and $\beta$ represent the copper and copper oxide regions, respectively. By substituting Eq. (30) into Eqs. (7), (8) and (10), we can obtain the radial, circumferential and axial stresses in the copper region as follows

$$\sigma_r^{\alpha} = \sigma_{\theta}^{\alpha} = \frac{E_{\alpha}}{(1-\nu)} C_1,\ \sigma_z^{\alpha} = \frac{2\nu E_{\alpha}}{(1-\nu)} C_1, \tag{31}$$

where the parameter $C_1$ is

$$C_1 = \frac{\Omega E_{\beta}\left(c^2 - b^2\right)(1-\nu)}{3\left\{(1-\nu)\left(E_{\beta} - E_{\alpha}\right)c^2 - \left[E_{\alpha}(1+\nu) + E_{\beta}(1-\nu)\right]b^2\right\}}.$$

The radial and circumferential strains in the copper region are

$$\varepsilon_r^{\alpha} = \varepsilon_{\theta}^{\alpha} = C_1. \tag{32}$$

The radial, circumferential and axial stresses in the copper oxide region are

$$\begin{aligned}
\sigma_r^{\beta} &= \frac{E_{\beta}}{1-\nu^2}\left[(1+\nu)C_2 - (1-\nu)\frac{C_3}{r^2}\right] - \frac{E_{\beta}}{1-\nu}\frac{\Omega}{3}, \\
\sigma_{\theta}^{\beta} &= \frac{E_{\beta}}{1-\nu^2}\left[(1+\nu)C_2 + (1-\nu)\frac{C_3}{r^2}\right] - \frac{E_{\beta}}{1-\nu}\frac{\Omega}{3}, \\
\sigma_z^{\beta} &= \frac{2\nu E_{\beta}}{1-\nu} C_2 - \frac{1+\nu}{1-\nu} E_{\beta}\frac{\Omega}{3},
\end{aligned} \tag{33}$$

where the parameters $C_2$ and $C_3$ are

$$\begin{aligned}
C_2 &= \frac{\Omega\left\{E_{\beta}(1-\nu)c^2 - \left[E_{\alpha}(1+\nu) + E_{\beta}(1-\nu)\right]b^2\right\}}{3\left\{(1-\nu)\left(E_{\beta} - E_{\alpha}\right)c^2 - \left[E_{\alpha}(1+\nu) + E_{\beta}(1-\nu)\right]b^2\right\}}, \\
C_3 &= \frac{\Omega E_{\alpha}(1+\nu)c^2 b^2}{3\left\{(1-\nu)\left(E_{\beta} - E_{\alpha}\right)c^2 - \left[E_{\alpha}(1+\nu) + E_{\beta}(1-\nu)\right]b^2\right\}}.
\end{aligned}$$

The radial and circumferential strains in the copper oxide region are

$$\varepsilon_r^{\beta} = C_2 - \frac{C_3}{r^2},\ \varepsilon_{\theta}^{\beta} = C_2 + \frac{C_3}{r^2}. \tag{34}$$

The elastic strain energy of the nanowire gradually accumulates with the interfacial movement. When the energy release rate $G$ reaches a critical value, the interlayer cracking occurs at the interface between copper region and copper oxide region. The expression of $G$ still follows the form of Eq. (22). Considering the distance between the crack and the center of nanowire is $c$, the strain energy of nanowire before interlayer cracking is

$$U_{\mathrm{e}} = 2\pi \int_0^c e_{\alpha}(r) r \mathrm{d}r + 2\pi \int_c^b e_{\beta}(r) r \mathrm{d}r, \tag{35}$$

where $e_\alpha$ and $e_\beta$ are the strain energy densities of copper region and copper oxide region before interlayer cracking, respectively. According to elastic mechanics, the strain energy densities $e_\alpha$ and $e_\beta$ under plane strain condition can be expressed as

$$e_\alpha(r) = \frac{1}{2}\left(\sigma_r^\alpha \varepsilon_r^\alpha + \sigma_\theta^\alpha \varepsilon_\theta^\alpha\right), \tag{36}$$

$$e_\beta(r) = \frac{1}{2}\left(\sigma_r^\beta \varepsilon_r^\beta + \sigma_\theta^\beta \varepsilon_\theta^\beta\right). \tag{37}$$

Substituting Eqs. (31)-(34) into Eqs. (36) and (37) yields

$$e_\alpha(r) = \frac{E_\alpha}{(1-\nu)} C_1^2, \tag{38}$$

$$e_\beta(r) = \frac{E_\beta}{1-\nu}\left(C_2 - \frac{\Omega}{3}\right)C_2 + \frac{E_\beta}{1+\nu}\frac{C_3^2}{r^4}. \tag{39}$$

By substituting Eqs. (38) and (39) into Eq. (35), the strain energy of nanowire $U_e$ is

$$U_e = 2\pi \cdot \left(\frac{E_\alpha}{1-\nu} C_1^2 c^2 + \frac{E_\beta}{1-\nu}\left(C_2 - \frac{\Omega}{3}\right)C_2 \cdot \frac{b^2-c^2}{2} + \frac{E_\beta}{1+\nu} C_3^2 \frac{b^2-c^2}{2c^2b^2}\right). \tag{40}$$

After the interlayer cracking, the strain energy of the system is the sum of strain energies of the copper and copper oxide regions, *i.e.*,

$$U_e^{'} = 2\pi \int_0^c e_\alpha^{'}(r) r \mathrm{d}r + 2\pi \int_c^b e_\beta^{'}(r) r \mathrm{d}r, \tag{41}$$

where $e_\alpha{}'$ and $e_\beta{}'$ are the strain energy densities of copper region and copper oxide regions, respectively. Additionally, both the radial displacement $\overline{u}_r^\alpha$ in the center of the copper region and the radial stress $\overline{\sigma}_r^\alpha$ on the surface are zero. As a result, the boundary conditions are

$$\overline{u}_r^\alpha|_{r=0} = 0,\ \overline{\sigma}_r^\alpha|_{r=c} = 0. \tag{42}$$

By considering the assumption of $\phi = 0$ in the copper region and then substituting Eq. (42) into Eqs. (7), (8) and (10), the radial stress $\overline{\sigma}_r^\alpha$, circumferential stress $\overline{\sigma}_\theta^\alpha$, axial stress $\overline{\sigma}_z^\alpha$, radial strain $\overline{\varepsilon}_r^\alpha$ and circumferential strain $\overline{\varepsilon}_\theta^\alpha$ in the copper region are

$$\overline{\sigma}_r^\alpha = \overline{\sigma}_\theta^\alpha = \overline{\sigma}_z^\alpha = 0,\ \overline{\varepsilon}_r^\alpha = \overline{\varepsilon}_\theta^\alpha = 0. \tag{43}$$

For the copper oxide region, the boundary conditions are

$$\overline{\sigma}_r^\beta|_{r=c} = \overline{\sigma}_r^\beta|_{r=b} = 0. \tag{44}$$

By considering the assumption of $\phi = 1$ in the copper oxide region and substituting Eq. (44) into Eqs. (7), (8) and (10), the radial stress $\overline{\sigma}_r^\beta$, circumferential stress $\overline{\sigma}_\theta^\beta$, axial stress $\overline{\sigma}_z^\beta$, radial strain $\overline{\varepsilon}_r^\beta$ and circumferential strain $\overline{\varepsilon}_\theta^\beta$ in the copper oxide region can be written as

$$\overline{\sigma}_r^\beta = \overline{\sigma}_\theta^\beta = 0,\ \overline{\sigma}_z^\beta = -\frac{E_\beta \Omega}{3},\ \overline{\varepsilon}_r^\beta = \overline{\varepsilon}_\theta^\beta = \frac{\Omega}{3}. \tag{45}$$

By using Eqs. (43) and (45), $e_\alpha{}'$ and $e_\beta{}'$ are

$$e_\alpha^{'}(r) = \frac{1}{2}\left(\overline{\sigma}_r^\alpha \overline{\varepsilon}_r^\alpha + \overline{\sigma}_\theta^\alpha \overline{\varepsilon}_\theta^\alpha\right) = 0, \tag{46}$$

$$e_\beta^{'}(r) = \frac{1}{2}\left(\overline{\sigma}_r^\beta \overline{\varepsilon}_r^\beta + \overline{\sigma}_\theta^\beta \overline{\varepsilon}_\theta^\beta\right) = 0. \tag{47}$$

Then the strain energy of the system is

$$U_e^{'} = 0. \tag{48}$$

By substituting Eqs. (40) and (48) into Eq. (22), the strain energy release rate $G$ of the interface is

$$G = \frac{E_\alpha}{1-\nu} C_1^2 c + \frac{E_\beta}{1-\nu}\left(C_2 - \frac{\Omega}{3}\right)C_2 \cdot \frac{b^2-c^2}{2c} + \frac{E_\beta}{1+\nu} C_3^2 \frac{b^2-c^2}{2c^3b^2}. \tag{49}$$

By considering the relation of $c = b - h$ and substituting Eq. (29) into Eqs. (49), $G$ can be rewritten as

$$G = \frac{E_\alpha}{1-\nu}\xi_1^2(b-\eta t) + \frac{E_\beta}{1-\nu}\left(\xi_2 - \frac{\Omega}{3}\right)\xi_2 \cdot \frac{2b\eta t - (\eta t)^2}{2(b-\eta t)} + \frac{E_\beta}{1+\nu}\xi_3^2 \frac{2b\eta t - (\eta t)^2}{2(b-\eta t)^3 b^2}, \tag{50}$$

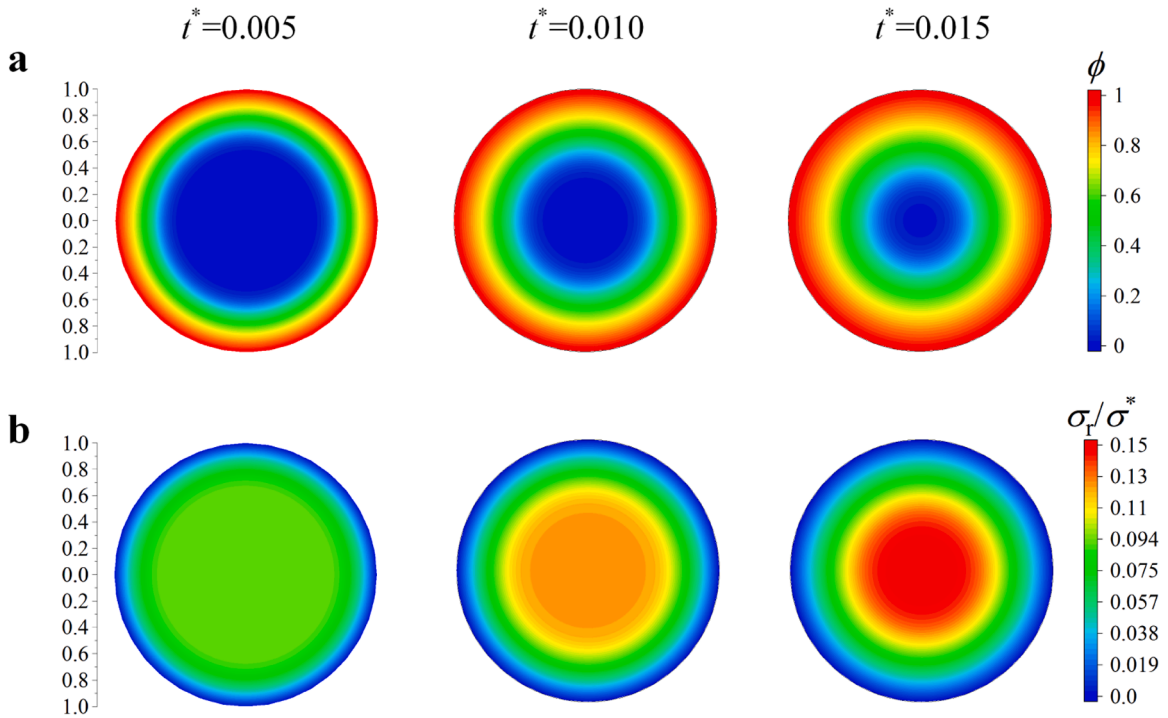


**Fig. 3.** (a) The distribution of oxygen concentration in the cross section of the copper nanowire under high oxygen for $t^* = 0.005$, 0.01 and 0.015 when $\zeta^* = 3$. (b) The distribution of radial stress in the cross section of the copper nanowire under high oxygen for $t^* = 0.005$, 0.01 and 0.015 when $\zeta^* = 3$.

where the parameters $\xi_1$, $\xi_2$ and $\xi_3$ are

$$\xi_1 = \frac{\Omega E_\beta\left(\eta^2 t^2 - 2b\eta t\right)(1-\nu)}{3\left\{2E_\alpha b^2 - 2(1-\nu)\left(E_\beta - E_\alpha\right)b\eta t + (1-\nu)\left(E_\beta - E_\alpha\right)(\eta t)^2\right\}},$$

$$\xi_2 = \frac{\Omega\left\{E_\beta(1-\nu)\left(\eta^2 t^2 - 2b\eta t\right) - E_\alpha(1+\nu)b^2\right\}}{3\left\{2E_\alpha b^2 - 2(1-\nu)\left(E_\beta - E_\alpha\right)b\eta t + (1-\nu)\left(E_\beta - E_\alpha\right)(\eta t)^2\right\}},$$

$$\xi_3 = \frac{\Omega E_\alpha(1+\nu)(b-\eta t)^2 b^2}{3\left\{2E_\alpha b^2 - 2(1-\nu)\left(E_\beta - E_\alpha\right)b\eta t + (1-\nu)\left(E_\beta - E_\alpha\right)(\eta t)^2\right\}}.$$

According to Eq. (50), we can obtain the energy release rate with time during the movement of the interface between the copper and copper oxide regions from the surface to the center of the nanowire.

In this Section, we have developed a chemo-mechanical coupling model to describe the oxidation and interlayer cracking behaviors of copper nanowire. This model combines the diffusion of oxygen ions in the nanowire with the oxidation of copper atoms and the volume expansion due to introduced oxygen. For the mechanical process, we consider the stress state of the nanowire to be in a static equilibrium while a combination of the diffusion behavior of oxygen ions induced by concentration gradient and the chemical reaction between oxygen and copper determines the chemical process. The interlayer cracking location during the oxidation of the nanowire is analyzed from energy release rate.

## 3. Results and discussion

### 3.1. Oxidation and interlayer cracking behaviors under high oxygen concentration

We first analyze the oxidation behavior of nanowires before interlayer cracking under high oxygen condition. The oxygen concentration $\phi$ is used to describe the oxidation behavior, which is associated with the following parameters: $\zeta$, $R$, $T$, $H$, $m$ and $\alpha$, and can be obtained through Eq. (20) with boundary conditions of Eq. (21). Since it is difficult to accurately identify these parameters, we introduce two dimensionless parameters, *i.e.*, $\zeta^* = \zeta/(RT)$ and $t^* = D_0 t/b^2$, to study the effects of the charge transfer $\zeta$ and reaction time $t$ on the oxidation behavior of nanowires. The dimensionless parameter $m$ is set as 0.45 by using Eq. (9) with Young's modulus of pure copper and copper oxide of 74 GPa and 107 GPa (Hui et al., 2020; Sondors et al., 2020). The Poisson's ratio of the namowire is taken as 0.34. In addition, we obtain the partial molar volume $\Omega$=0.74 based on the lattice constants of copper and copper oxide, i.e., 3.61 Å,

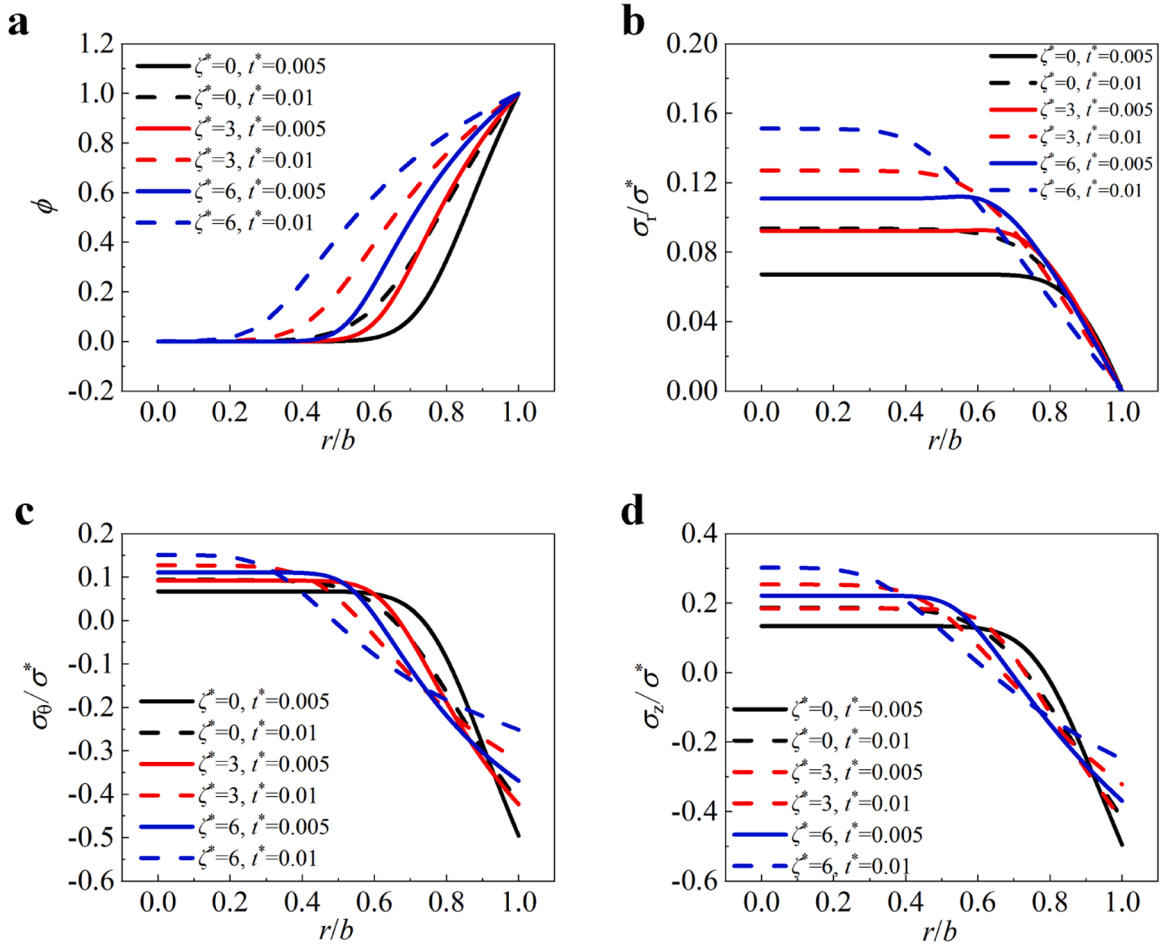


**Fig. 4.** (a) The distribution of oxygen concentration along the radial direction in the copper nanowire for $\zeta^* = 0$, 3 and 6 and $t^* = 0.005$ and 0.01, where $\zeta^* = \zeta/(RT)$ and $t^* = D_0 t/b^2$. The distributions of (b) radial, (c) circumferential and (d) axial stresses in the nanowire when $\zeta^* = 0$, 3 and 6 and $t^* = 0.005$ and 0.01.

3.61 Å, 3.61 Å (pure copper) and 4.69 Å, 3.43 Å, 5.10 Å (copper oxide). Moreover, we take $HE_0 = 0.2$ and $\alpha = 0.95$ and consider the constant environmental temperature during the oxidation process. We next use several color nephogram to visualize the distribution of oxygen concentration and radial stress in the cross-section of the nanowire. Fig. 3a shows the distribution of oxygen concentration in the cross section of the nanowire under high oxygen for $t^* = 0.005$, 0.01 and 0.015 when $\zeta^* = 3$. The evolution of oxygen concentration in the radial direction are indicated by the color contours, with red region representing the copper oxide and blue region the copper. As $t^*$ increases from 0.005 to 0.015, the oxygen concentration in the nanowire increases, implying that oxidation advances in the nanowire gradually. Fig. 3b shows the distribution of radial stress $\sigma_r/\sigma^*$ in the cross section of the nanowire for $t^* = 0.005$, 0.01 and 0.015 where $\sigma^* = \Omega E_0/(3-3\nu)$. The radial stress monotonically decreases from the maximum value to zero along the radial direction due to the volume expansion of copper oxide, which generates tensile stress in the copper oxide region and the inner copper region.

Fig. 4a further shows the distribution of oxygen concentration along the radial direction in the nanowire for several values of $\zeta^*$ and $t^*$. It is seen that the oxygen concentration in the nanowire increases with $\zeta^*$. Furthermore, a large $\zeta^*$ corresponding to a high reaction rate leads to a large area of copper oxide. These findings demonstrate that increasing the reaction time and temperature can enhance the oxidation of copper nanowire.

The oxidation of copper nanowire induces volume expansion and subsequent internal stress. For simplicity, we define the dimensionless parameters of $\sigma_r/\sigma^*$, $\sigma_\theta/\sigma^*$ and $\sigma_z/\sigma^*$ to describe the stress distribution in the nanowire, in which $\sigma^* = \Omega E_0/(3-3\nu)$. As shown in Figs. 4b-d, the radial, circumferential and axial stresses in the nanowire are calculated by using Eq. (12) with the values of $\phi$ shown in Fig. 4a. As $t^*$ and $\zeta^*$ increase, the radial stress near the center gradually increases while the one near the surface slightly decreases. The increase in the radial stress near the center is contributed to the accumulation of tensile stresses toward the center region induced by a large copper oxide region and volume expansion corresponding to high $t^*$ and $\zeta^*$. For the circumferential stress, the volume expansion in the copper oxide region results in the compressive stress along the circumferential direction near the surface of the nanowire and tensile stress near the center. As $t^*$ and $\zeta^*$ increase, the nanowire gradually expands. The existed copper oxide region is pushed outwards by the newly oxidized region. The volume expansion near the surface is inevitably. Therefore, the existing

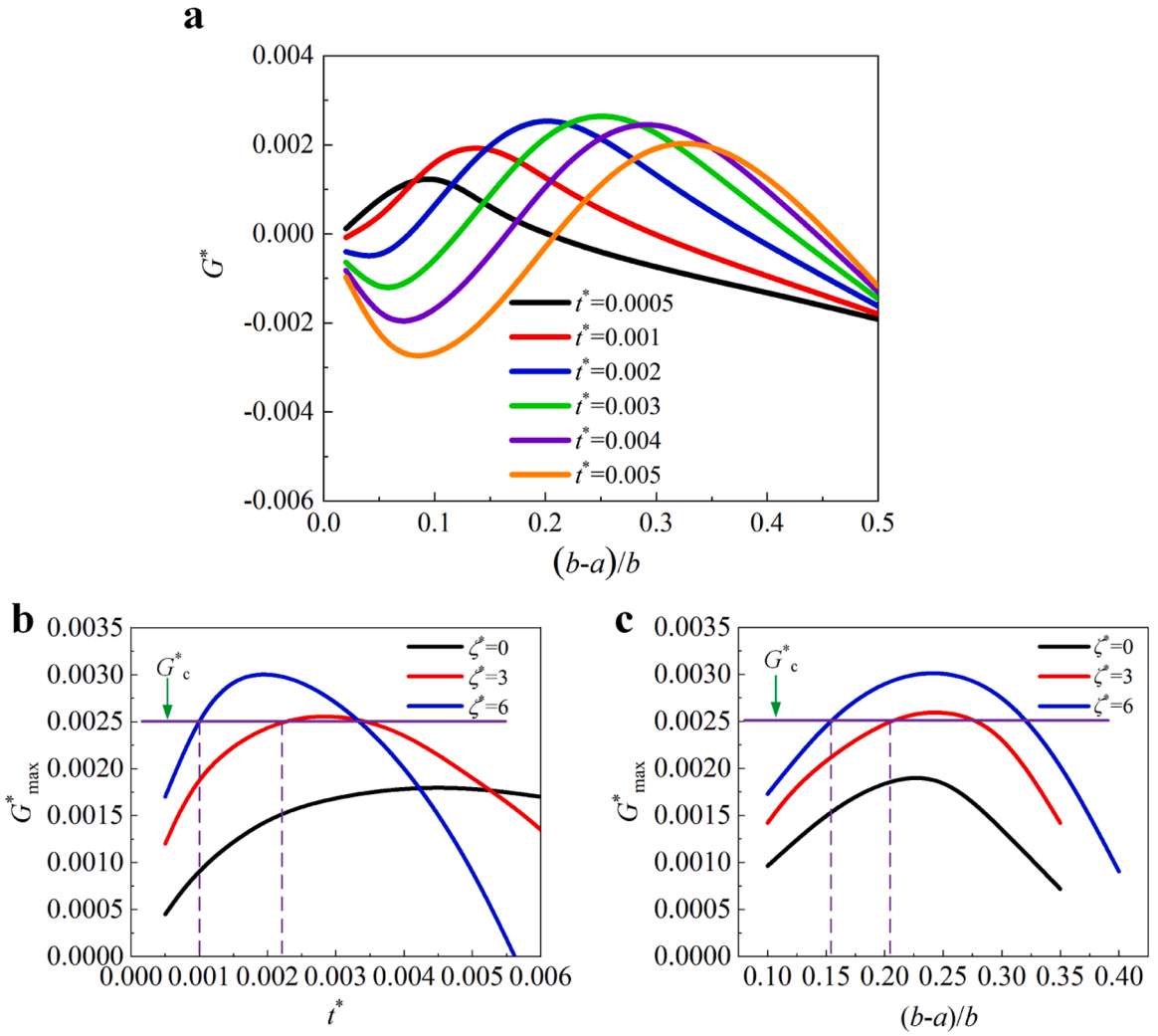


**Fig. 5.** (a) The variation of the energy release rate $G^*$ with respect to the location in the radical direction of nanowire under several $t^*$ when $\zeta^* = 3$. The variations of the maximum energy release rate $G^*_{max}$ with respect to (b) the oxidation time $t^*$ and (c) radial location of the interlayer cracking $(b-a)/b$ in the nanowire. For any $G^*_{max}$, we can obtain the oxidation time from Fig. 5b and the corresponding radial location of the interlayer cracking from Fig 5c.

copper oxide region is pushed outwards by the newly oxidized region. The volume expansion near the surface is inevitable. Moreover, the circumferential tensile stress near the center increases with the radial stress. The trend of axial stress is exactly the same as that of circumferential stress.

After determining the stress distribution in the nanowire during the oxidation process, we now analyze its interlayer cracking behavior. Along with previous analysis, we cannot directly obtain both the location of interlayer cracking and the corresponding energy release rate of nanowire. In this case, we consider that the interlayer cracking occurs at an arbitrary location along the radial direction with a specific oxidation time and then calculate the energy release rate of nanowire by using Eq. (55) with relevant parameters. To determine the location of interlayer cracking, we will study the oxidation-fracture processes of nanowire under specific reaction conditions. The location with the maximum strain energy release rate is regarded as the location where the interlayer cracking is most likely to occur. Similarly, we define a dimensionless parameter $G^* = (3-3\nu)G/(\Omega E_0 b)$ to describe the energy release rate. Fig. 5a shows the variation of the energy release rate with respect to the location along the radial direction of nanowire under several values of $t^*$ when $\zeta^* = 3$. For simplicity, $(b-a)/b$ is used to describe the location along the radial direction. When $(b-a)/b > 0.5$, the obtained energy release rates have a negative value, indicating that the interlayer cracking cannot occur at these locations. Hence, these values are not shown in Fig. 5a. For a certain $t^*$, the curve of $G^*$ is non-monotonic and has maximum value with respect to the location along the radial direction. For any $t^*$, the location with the maximum energy release rate lies in the transition region between copper and copper oxide, indicating the interlayer cracking may occur in such location. As $t^*$ increases, the location with the maximum energy release rate moves from the surface to the center of nanowire. Figs. 5b and 5c show the variations of the maximum energy release rate $G^*_{max}$ with respect to the oxidation time $t^*$ and radial location $(b-a)/b$ under several values of $\zeta^*$, respectively. There exists a certain

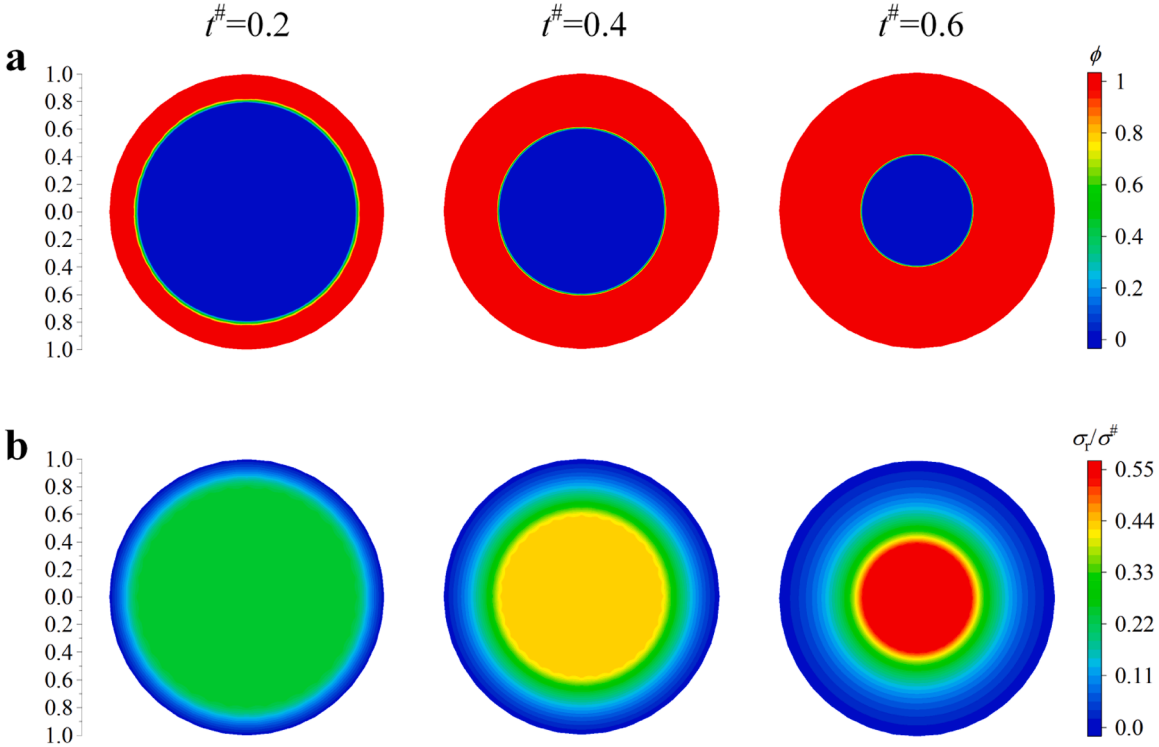


**Fig. 6.** (a) The distribution of oxygen concentration in the cross section of the copper nanowire under low oxygen for $t^{\#} = 0.2$, 0.4 and 0.6. (b) The distribution of radial stress in the cross section of the copper nanowire under low oxygen for $t^{\#} = 0.2$, 0.4 and 0.6.

correlation between the oxidation time and the location corresponding to $G^*_{max}$. Therefore, $G^*_{max}$ has the same trend with the variation of these two parameters, *i.e.*, at an oxidation process $G^*_{max}$ first increases then decreases with increasing $(b-a)/b$ and $t^*$. Theoretically, there is only one location where the interlayer cracking occurs along the radial direction during this process. For simplicity, we consider the critical energy release rate $G^*_c$ of a nanowire as a constant along the radial direction, *e.g.*, $G^*_c = 0.0025$. When $G^*_{max}$ reaches the value of $G^*_c$, the interlayer cracking occurs at a location along the radial direction. From Fig. 5c, it can also be found that $G^*_{max}$ gradually increases at the same location as $\zeta^*$ increases. It demonstrates that a larger value of $\zeta^*$ corresponding to a higher reaction rate results in more strain energy accumulation in the nanowire, thus favors the interlayer cracking. In addition, as the value of $\zeta^*$ increases, the interlayer cracking occurs at a location closer to the surface of nanowire. When $\zeta^* = 0$, $G^*_{max}$ is lower than $G^*_c$ in the entire radial range, thus the interlayer cracking of nanowire cannot occur.

### 3.2. Oxidation and interlayer cracking behaviors under low oxygen concentration

As previously mentioned, the copper nanowire is oxidized layer-by-layer from outside to inside under low oxygen condition. There exist two distinct regions, *i.e.,* copper oxide and pure copper regions, in the entire oxidation process. To describe the stress distributions in the two regions along three principal directions of nanowire, we define three dimensionless parameters $\sigma_r/\sigma^{\#}$, $\sigma_\theta/\sigma^{\#}$ and $\sigma_z/\sigma^{\#}$, in which $\sigma^{\#} = \Omega E_\alpha/3$. Moreover, we use the dimensionless parameter $t^{\#} = \eta t/b$ to describe the reaction time. The parameters $E_\alpha/E_\beta$ and $\nu$ are taken as 1.45 and 0.34, respectively Tan et al., 2007). The stress distributions in the copper and copper oxide regions can be calculated by using Eqs. (31) and ((33). Fig. 6a shows the distribution of oxygen concentration in the cross section of the nanowire under low oxygen for $t^{\#} = 0.2$, 0.4 and 0.6. The evolution of oxygen in the radial direction are indicated by the color contours. In contrast to the case of high oxygen, there is no transition region between the copper and copper oxide regions. In this process, the interface between copper oxide and copper regions in the nanowire moves gradually from surface to center. Fig. 6b shows the distribution of radial stress $\sigma_r/\sigma^{\#}$ in the cross section of the nanowire under low oxygen for $t^{\#} = 0.2$, 0.4 and 0.6. The radial stress in the copper region has a constant value while in the copper oxide region, it gradually decreases along the radial direction. As $t^{\#}$ increases, the radial stress increases in the copper region while decreases in the copper oxide region.

Figs. 7a-7c further show the distributions of the radial, circumferential and axial stresses in the nanowire under several values of $t^{\#}$. The volume expansion of the copper oxide region results in compressive stress along circumferential and axial directions in the copper oxide region and tensile stress in the copper region. As time increases, the circumferential and axial stresses increase in the copper region and decrease in the copper oxide region. As the oxidation reaction advances, the volume of copper oxide region gradually expands and the strain energy in the nanowire increases. When the interfacial energy release rate between copper oxide and copper regions reaches its critical value, the interlayer cracking of nanowire occurs at the interface. Similar as the previous analysis, we

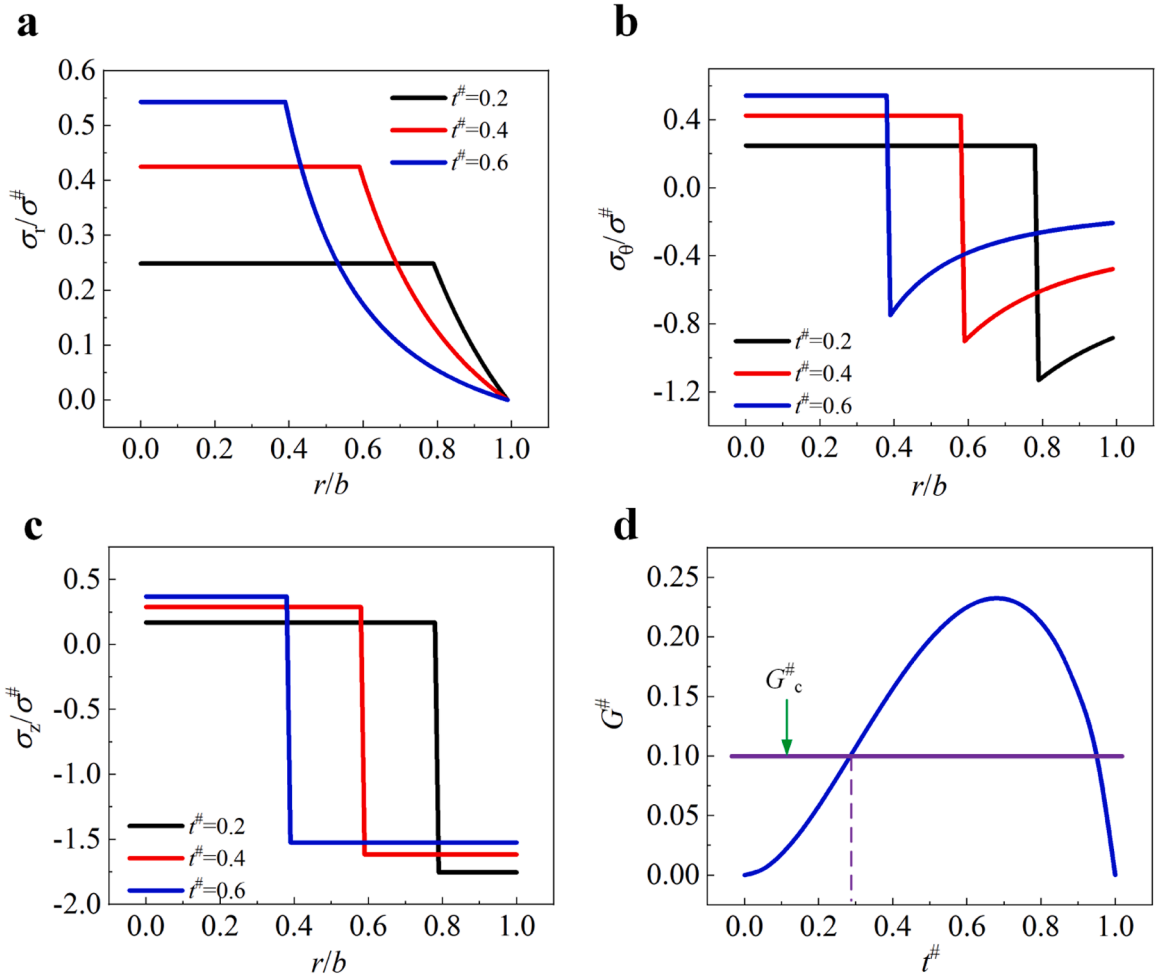


**Fig. 7.** The distributions of (a) radial, (b) circumferential and (c) axial stresses in the nanowire for $t^{\#} = 0.2$, 0.4 and 0.6. (d) The variation of the energy release rate $G^{\#}$ with respect to the oxidation time $t^{\#}$.

consider the interlayer cracking occurs at an arbitrary location along the radial direction with a specific oxidation time. The interfacial energy release rate between two regions can be calculated by using Eq. (50). The dimensionless parameter $G^{\#} = 9G/(\Omega^2 E_\alpha b)$ is defined to describe the interfacial energy release rate. Fig. 7d shows the variation of $G^{\#}$ with respect to the oxidation time $t^{\#}$. According to Eq. (29), there exists a positive correlation between the interfacial location and the oxidation time. The interfacial energy release rate first increases then decreases with increasing $t^{\#}$ under low oxygen condition. Let $G_c^{\#}$ denote the critical energy release rate of the interface which has a constant value along the radical direction of nanowire. For the nanowire with a larger value of $G_c^{\#}$, it takes longer oxidation time for the occurrence of interlayer cracking, and the location is closer to its center.

## 4. Molecular dynamics simulation of the oxidation behavior of copper

In the previous Sections, we have set up a theoretical model to describe the oxidation of copper nanowire in which the diffusion of oxygen ions is presumed. However, the underneath mechanism of how the oxygen ions diffuse is still unclear. To clarify the effects of the reaction between the copper and oxygen ions and the diffusion of the oxygen ions in the chemical process, as well as the reaction path of oxygen ions within the copper crystals, we conduct molecular dynamics simulations of the oxidation process in the conditions with and without charge transfer, respectively.

### 4.1. Molecular dynamics simulation model

LAMMPS is used for molecular dynamics simulations of the oxidation behavior of copper (Plimpton, 1995). We construct a model with dimensions of 36.15 Å × 36.15 Å × 51.83 Å, which consists of a 31.83 Å copper layer with 3200 copper atoms and a 20 Å vacuum layer in $z$ direction, as shown in Fig. 8a. The (100) surface of copper is selected. All the simulations are carried out at an elevated temperature of 623 K with periodic boundary condition in $x$ and $y$ directions. A time step of 1 fs is used for all calculations. 400 oxygen

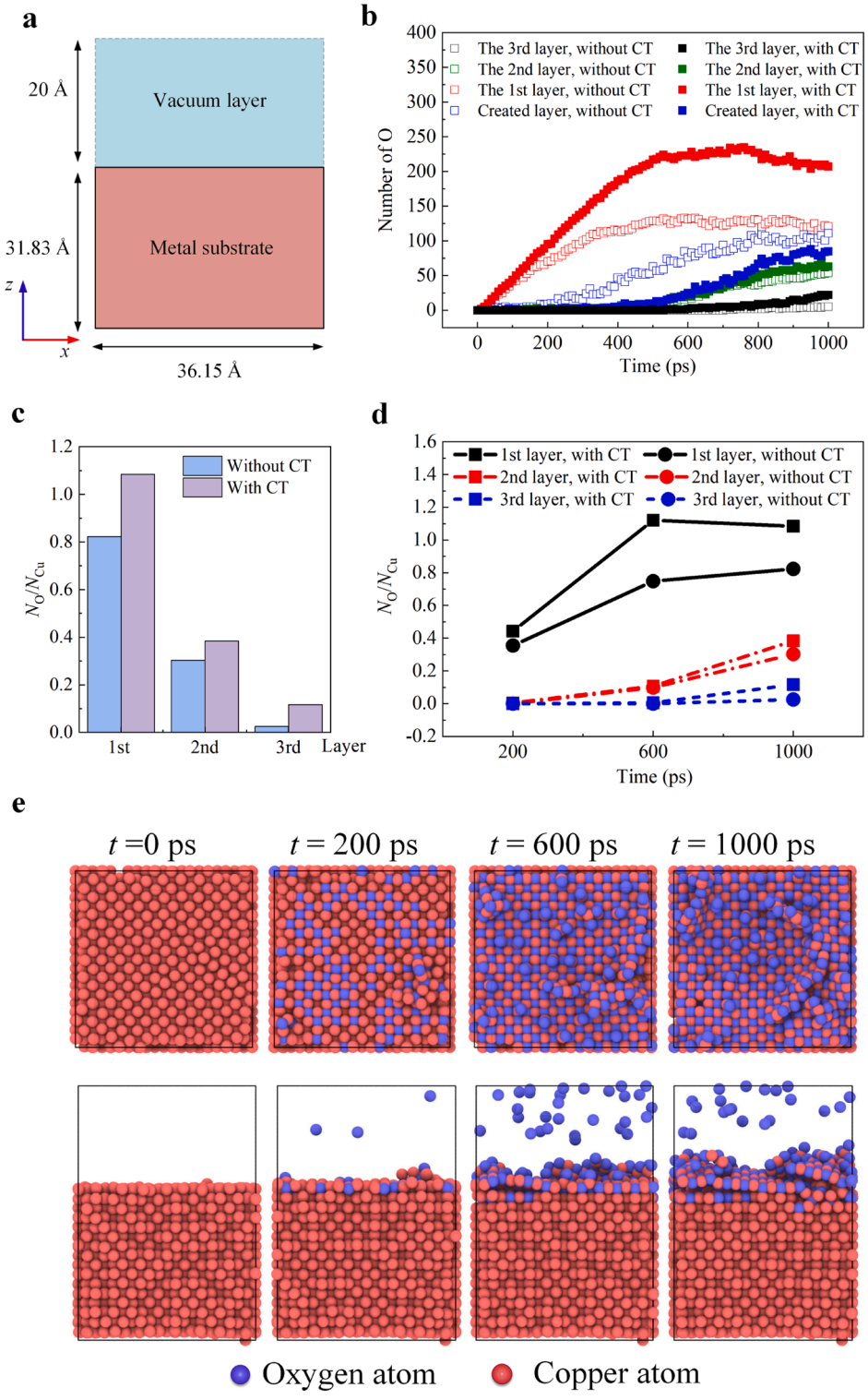


**Fig. 8.** (a) Schematic of the atomistic simulation model. (b) The number of oxygen ions entering the different layers with and without charge transfer. (c) Oxygen concentration in each layer at 1000 ps. (d) Oxygen concentration in each layer at 200 ps, 600 ps and 1000 ps. (e) Top and side views of the oxidation process from 0 to 1000 ps with charge transfer. The red and blue spheres represent copper atoms and oxygen atoms, respectively.

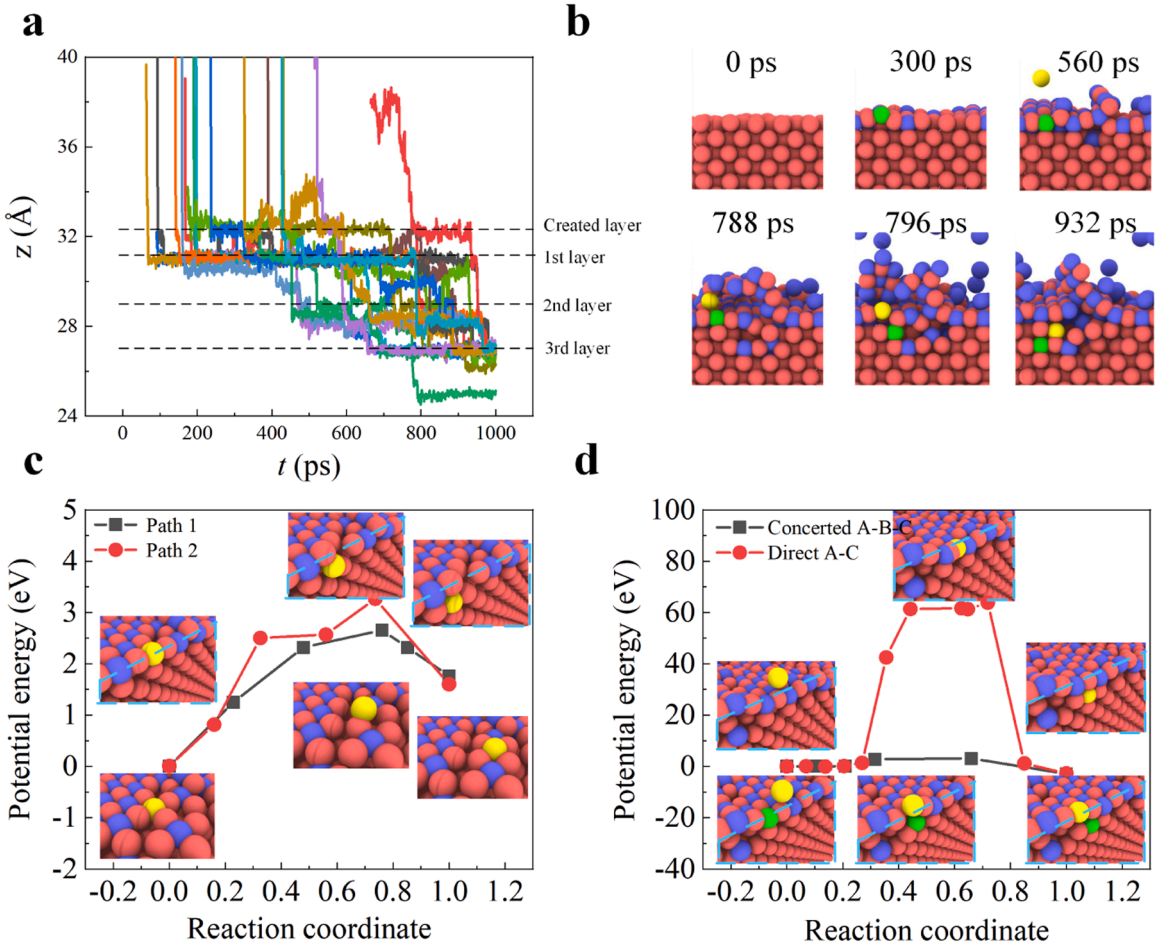


**Fig. 9.** (a) Trajectory diagram of oxygen ions entering the second layer. (b) After the oxygen ions (blue color) gradually spread over the first layer, they (green color) start to enter into the second and third layer with their original position filled by new oxygen ions (yellow color). (c) Potential energy changes of lateral movement of oxygen ion in the first layer (black dots) and inward movement of oxygen ion when the first layer is not fully filled with oxygen ions (red dots). (d) Potential energy change of inward movement of oxygen ion in the first layer with its initial position filled by another oxygen ion (black dots, co-diffusion) and inward movement of oxygen ion in vacuum passing through the first layer filled with other oxygen ions and entering the second layer (red dots, direct diffusion).

ions are filled into the vacuum layer one by one at 2 ps interval. The entire process is carried out under an NVT ensemble for 1000 ps. The reaxFF potential (Byoungseon et al., 2011) is adopted to simulate the oxidation process of copper. To quantitatively describe the effect of chemical reaction of copper and oxygen atoms on the oxidation process of copper layer, we simulate the oxidation process of the copper layer with and without charge transfer (CT). When the CT is considered, the charge distribution will be calculated during MD simulation with the help of ReaxFF potential which will consider the bonding and debonding during oxidation. However, if CT is not included, it means there is no oxidation process and the main driving force of the movement of oxygen ions is only related to their concentration gradient. The number of oxygen ions that enter the copper layer is used to evaluate the degree of oxidation of copper.

### *4.2. Oxidation characteristics of copper surface*

We have studied the oxidation process until 1000 ps and compared the number of oxygen ions entering different layers with and without CT, as shown in Fig. 8b. Fig. 8c shows the oxygen concentration to the copper atoms in each layer at steady state with and without CT at 1000 ps. We find that with the CT, the number of oxygen ions entering the first layer, the second layer, the third layer and the total number of oxygen ions involved in the reaction are significantly higher than that without CT (Fig. 8b). This indicates that the CT (oxidation reaction) could accelerate the diffusion of oxygen ions. It is worth noting that on the newly created copper atomic layer where the copper atoms are initially located in the first atomic layer, the results are reversed. It indicates that the charge transfer promotes the diffusion of oxygen ions driven by the gradient of chemical potential, resulting in more oxygen ions entering the inside of copper. In Figure 8d, we show the variation of oxygen concentration in each layers with time with and without CT. We find that the oxygen concentration gradually increases with time, implying that the oxidation reaction advances toward the inside of the copper.

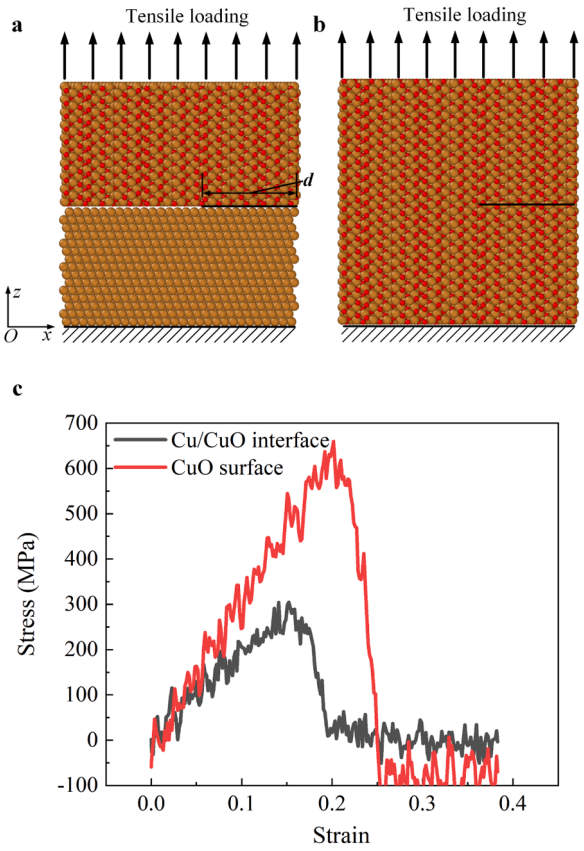


**Fig. A.1.** Schematic illustration of the simulated model with an edge crack. Atomic configurations of (a) interface of Cu and CuO, (b) surface of CuO. The brown and red spheres represent copper and oxygen atoms, respectively. (c) Stress-strain curves of simulated samples.

This conclusion is in full agreement with our theoretical results. Furthermore, the oxygen concentration with CT is higher than that without CT, which illustrate that CT facilitates the diffusion of oxygen. Therefore, the effect of chemical reactions is considered in our chemo-mechanical coupling model.

The snapshots (top and side views) of the oxidation process from 0 to 1000 ps for the case of CT are shown in Fig. 8e. During the initial period of the oxidation reaction ($t < 200$ ps), the oxygen ions gradually fall into the hollow sites between the four copper atoms. A small number of copper atoms are squeezed out of the first copper layer. As the reaction continues, the oxygen ions gradually fill the hollow sites between the copper atoms in the first layer and more copper atoms are squeezed out of the first layer to form a newly layer of copper atoms. As the oxygen ions fill the gaps in the first layer of copper atoms, the oxygen ions gradually diffuse into the second layer.

To further elucidate the diffusion pathway of the oxygen ions during the oxidation reaction, we plot the variation of z coordinates of the oxygen ions entering the third layer in Fig. 9a. We can see that all the oxygen ions enter into the first layer and stay there for a while, then further enter into the second layer. This phenomenon indicates that the oxygen ions in the first layer would enter the second and third layer when they are firstly spread over the first layer, rather than entering across the second layer directly from the vacuum. The zoom-in view of the pathway is shown in Fig. 9b that as the oxygen ions spread over the first layer, one oxygen ion that was previously in the first layer (green sphere) enters the second layer and its original position is replaced by another one from vacuum (yellow sphere). Then, driven by the subsequent oxygen ions, the green sphere enters the third layer and the original position of the second layer is once again replaced by the yellow sphere. We expect this replacement would occur further in the third, fourth *etc* layers, eventually exhibiting a diffusion process of oxygen ions. In contrast to commonly known direct diffusion of atoms in crystalline materials that the diffused atom would not occupy the lattice point, here the oxygen ions would replace and occupy the lattice points during diffusion, which we define it as co-diffusion. It is expected such co-diffusion would be energetic favorable. To verify it, we evaluate the energy barrier of the oxygen ions during the diffusion using nudged elastic band (NEB) method (Henkelman and Jónsson, 2000; Henkelman et al., 2000). Fig. 9c shows the potential energy changes of lateral movement of oxygen ion in the first layer (black dots) and inward movement of oxygen ion when the first layer is not fully filled with oxygen ions (red dots). The results show that the energy barrier of lateral movement of oxygen ions on the surface is slightly smaller than that of the inward movement (Fig. 9c). Fig. 9d shows the potential energy change of inward movement of oxygen ion in the first layer with its initial position filled by another oxygen ion (black dots, co-diffusion) and inward movement of oxygen ion in vacuum passing through the first layer filled with other oxygen

ions and entering the second layer (red dots, direct diffusion). It is seen that the energy barrier of direct diffusion (63.8 eV) is much higher than that of co-diffusion (3.12 eV). It demonstrates that oxygen ions in the outer layer do not cross over the oxygen atoms in the inner layer during their entry. Combined with the effect of chemical reactions on the diffusion of oxygen ions in copper nanowires shown in Fig. 8, this particular diffusion mechanism is called chemical reaction-mediated layer-by-layer replacement.

## 5. Conclusion

In this paper we develop a chemo-mechanical coupling model for the oxidation of copper nanowires. In contrast to existing chemo-mechanical models, this model emphasizes the mechanism that oxygen ion enters the copper nanowires in a reaction-driven cascade-like manner rather than vacancy-mediated diffusion. Under the assumption of small deformation and plane strain, the mechanics and diffusion equations for homogeneous metallic copper nanowire are derived. By solving the control equations with initial and boundary conditions, we obtain the oxygen concentration and various stress states. The diffusion pathway of oxygen ions during copper oxidation is also studied via an atomic simulation. We find that the radial stress dominates the fracture of the copper nanowire through interlayer cracking, which occurs when the energy release rate reaches a critical value. The relationship between the fracture location and the parameter of chemical reaction is obtained to elucidate the oxidation behavior of copper. It could be extended to understand the oxidation of other metals and alloys, and provide a theoretical basis for future corrosion prevention.

## CRediT authorship contribution statement

**Yulong Gong:** . **Xin Yan:** . **Jici Wen:** . **Qinghua Meng:** . **Ang Li:** Conceptualization. **Xinghua Shi:** Conceptualization, Writing – review & editing, Funding acquisition, Project administration.

## Declaration of Competing Interest

The authors declare that they have no known competing financial interests or personal relationships that could have appeared to influence the work reported in this paper.

## Data availability

Data will be made available on request.

## Acknowledgments

We are grateful for financial support from the Strategic Priority Research Program of Chinese Academy of Sciences (XDB36000000), the National Natural Science Foundation of China (12072082), the National Natural Science Foundation for Distinguished Young Scholars of China (12125202).

## Appendix A. The expression of the energy release rate G under high oxygen condition

After the interlayer cracking in the nanowire, the boundary conditions of copper nanowire are

$$u_r^i|_{r=0} = 0,\ \sigma_r^i|_{r=a} = 0, \tag{51}$$

where $u_r^i$ is the radial displacement of the copper nanowire. Substituting Eq. (28) into Eq. (10) yields

$$\begin{aligned}
\sigma_r^i &= \frac{\Omega E}{3(1-\nu)}\left[\frac{1}{a^2}\int_0^a \phi(r) r\mathrm{d}r - \frac{1}{r^2}\int_0^r \phi(r) r\mathrm{d}r\right],\\
\sigma_\theta^i &= \frac{\Omega E}{3(1-\nu)}\left[\frac{1}{a^2}\int_0^a \phi(r) r\mathrm{d}r + \frac{1}{r^2}\int_0^r \phi(r) r\mathrm{d}r - \phi(r)\right],\\
\sigma_z^i &= \frac{\Omega E}{3(1-\nu)}\left[\frac{2}{a^2}\int_0^a \phi(r) r\mathrm{d}r - \phi(r)\right].
\end{aligned} \tag{52}$$

Moreover, the boundary conditions of hollow nanotube are

$$\sigma_r^o|_{r=a} = 0,\ \sigma_r^o|_{r=b} = 0. \tag{53}$$

Then, by substituting Eq. (30) into Eqs. (7), (8) and (10), the stress distributions in the hollow nanotube can be written as

$$\sigma_r^o = \frac{\Omega E}{3(1-\nu)}\left[\frac{r^2-a^2}{r^2\left(b^2-a^2\right)}\int_a^b \phi(r) r\mathrm{d}r - \frac{1}{r^2}\int_a^r \phi(r) r\mathrm{d}r\right],$$
$$\sigma_\theta^o = \frac{\Omega E}{3(1-\nu)}\left[\frac{r^2+a^2}{r^2\left(b^2-a^2\right)}\int_a^b \phi(r) r\mathrm{d}r + \frac{1}{r^2}\int_a^r \phi(r) r\mathrm{d}r - \phi(r)\right], \tag{54}$$
$$\sigma_z^o = \frac{\Omega E}{3(1-\nu)}\left[\frac{1}{b^2-a^2}\int_a^b \phi(r) r\mathrm{d}r - \phi(r)\right].$$

By substituting Eqs. (14), (25)-(29), (31), (33) into Eq. (24), the energy release rate $G$ can be obtained

$$\begin{aligned}
G = {} & 2\pi\int_0^b \frac{\Omega^2E^2}{9(1-\upsilon)^2}\left\{\frac{1}{2E}\left[\left(\frac{1}{b^2}\int_0^b \phi r\mathrm{d}r - \frac{1}{r^2}\int_0^r \phi r\mathrm{d}r\right)^2 + \left(\frac{1}{b^2}\int_0^b \phi r\mathrm{d}r + \frac{1}{r^2}\int_0^r \phi r\mathrm{d}r - \phi\right)^2\right.\right. \\
& \left.\left. + \left(\frac{2}{b^2}\int_0^b \phi r\mathrm{d}r - \phi\right)^2\right] - \frac{\nu}{E}\left[\left(\frac{1}{b^2}\int_0^b \phi r\mathrm{d}r - \frac{1}{r^2}\int_0^r \phi r\mathrm{d}r\right)\cdot\left(\frac{1}{b^2}\int_0^b \phi r\mathrm{d}r + \frac{1}{r^2}\int_0^r \phi r\mathrm{d}r - \phi\right)\right. \\
& + \left(\frac{1}{b^2}\int_0^b \phi r\mathrm{d}r + \frac{1}{r^2}\int_0^r \phi r\mathrm{d}r - \phi\right)\cdot\left(\frac{2}{b^2}\int_0^b \phi r\mathrm{d}r - \phi\right) \\
& \left.\left. + \left(\frac{2}{b^2}\int_0^b \phi r\mathrm{d}r - \phi\right)\cdot\left(\frac{1}{b^2}\int_0^b \phi r\mathrm{d}r - \frac{1}{r^2}\int_0^r \phi r\mathrm{d}r\right)\right]\right\} r\mathrm{d}r \\
& - 2\pi\int_0^a \frac{\Omega^2E^2}{9(1-\upsilon)^2}\left\{\frac{1}{2E}\left[\left(\frac{1}{a^2}\int_0^a \phi r\mathrm{d}r - \frac{1}{r^2}\int_0^r \phi r\mathrm{d}r\right)^2 + \left(\frac{1}{a^2}\int_0^a \phi r\mathrm{d}r + \frac{1}{r^2}\int_0^r \phi r\mathrm{d}r - \phi\right)^2\right.\right. \\
& \left.\left. + \left(\frac{2}{a^2}\int_0^a \phi r\mathrm{d}r - \phi\right)^2\right] - \frac{\nu}{E}\left[\left(\frac{1}{a^2}\int_0^a \phi r\mathrm{d}r - \frac{1}{r^2}\int_0^r \phi r\mathrm{d}r\right)\cdot\left(\frac{1}{a^2}\int_0^a \phi r\mathrm{d}r + \frac{1}{r^2}\int_0^r \phi r\mathrm{d}r - \phi\right)\right. \\
& + \left(\frac{1}{a^2}\int_0^a \phi r\mathrm{d}r + \frac{1}{r^2}\int_0^r \phi r\mathrm{d}r - \phi\right)\cdot\left(\frac{2}{a^2}\int_0^a \phi r\mathrm{d}r - \phi\right) \\
& \left.\left. + \left(\frac{2}{a^2}\int_0^a \phi r\mathrm{d}r - \phi\right)\cdot\left(\frac{1}{a^2}\int_0^a \phi r\mathrm{d}r - \frac{1}{r^2}\int_0^r \phi r\mathrm{d}r\right)\right]\right\} r\mathrm{d}r \\
& - 2\pi\int_a^b \frac{\Omega^2E^2}{9(1-\nu)^2}\left(\frac{1}{2E}\left[\left(\frac{r^2-a^2}{r^2\left(b^2-a^2\right)}\int_a^b \phi r\mathrm{d}r - \frac{1}{r^2}\int_a^r \phi r\mathrm{d}r\right)^2\right.\right. \\
& + \left(\frac{r^2+a^2}{r^2\left(b^2-a^2\right)}\int_a^b \phi r\mathrm{d}r + \frac{1}{r^2}\int_a^r \phi r\mathrm{d}r - \phi\right)^2 + \left(\frac{1}{b^2-a^2}\int_a^b \phi r\mathrm{d}r - \phi\right)^2 \\
& - \frac{\nu}{E}\left\{\left[\frac{r^2-a^2}{r^2\left(b^2-a^2\right)}\int_a^b \phi r\mathrm{d}r - \frac{1}{r^2}\int_a^r \phi r\mathrm{d}r\right]\cdot\left[\frac{r^2+a^2}{r^2\left(b^2-a^2\right)}\int_a^b \phi r\mathrm{d}r + \frac{1}{r^2}\int_a^r \phi r\mathrm{d}r - \phi\right]\right. \\
& + \left[\frac{r^2+a^2}{r^2\left(b^2-a^2\right)}\int_a^b \phi r\mathrm{d}r + \frac{1}{r^2}\int_a^r \phi r\mathrm{d}r - \phi\right]\cdot\left[\frac{1}{b^2-a^2}\int_a^b \phi r\mathrm{d}r - \phi\right] \\
& \left.\left.\left. + \left[\frac{1}{b^2-a^2}\int_a^b \phi(r) r\mathrm{d}r - \phi(r)\right]\cdot\left[\frac{r^2-a^2}{r^2\left(b^2-a^2\right)}\int_a^b \phi(r) r\mathrm{d}r - \frac{1}{r^2}\int_a^r \phi(r) r\mathrm{d}r\right]\right\}\right) r\mathrm{d}r.
\end{aligned} \tag{55}$$

Given the crack location $a$, we can obtain the energy release rate $G$ at this crack location by substituting it into Eq. (55).

## Appendix B. The comparison of fracture toughness of Cu/CuO and CuO

To compare the toughness of the interface of Cu/CuO and the surface of copper oxide, we conduct additional molecular dynamics simulations to explore the processes of crack growth at the interface and surface. LAMMPS is used for molecular dynamics simulations of the oxidation behavior of copper (Plimpton, 1995). We construct a model with dimensions of 61.72 Å × 25.56 Å × 143.14 Å, which consists of a 62.67 Å CuO and Cu layer with 2516 O atoms and 6784 Cu atoms and a 87.47 Å vacuum layer in z direction, as shown in Fig. A.1a. The Cu/CuO interface is prepared as follows: (1) building the lowest energy surface for Cu (111) and CuO (010), respectively (Tafreshi et al., 2015; Su et al., 2014); (2) matching the lattice of Cu (111) and CuO (010); (3) expanding the cell to get the complete model. The atomic configuration of the CuO surface consists of 5168 oxygen atoms and 5168 copper atoms, as shown in Fig. A1b. A time step of 0.5 fs is used for all calculations. The reaxFF potential (Byoungseon et al., 2011) is adopted to simulate the loading process of samples.

To quantify the toughness of the Cu/CuO interface and the CuO surface, a tensile load is applied vertically upwards to the top of the CuO layer. The tensile rate is 0.0002 Å/fs. An initial sharp edge crack with a length of 21.75 Å is introduced in the middle of the sample

by eliminating the interaction across the crack surfaces. The entire process is carried out under an NVE ensemble for 120 ps. We have investigated the relationship between the tensile loading and displacement in tension of the simulated samples as shown in Fig. A1c. We find that the CuO surface could bear higher tensile loading before fracture than the interface of Cu/CuO. Furthermore, the toughness of the CuO surface is much higher than the Cu/CuO interface.

## References


Anand, L., 2012. A Cahn-Hilliard-type theory for species diffusion coupled with large elastic-plastic deformations. J. Mech. Phys. Solids 60 (12), 1983–2002.

Byoungseon, J., Subramanian, K.R.S., Sankaranarayanan, Adri C.T., van Duin, Shriram, R., 2011. Influence of surface orientation and defects on early-stage oxidation and ultrathin oxide growth on pure copper. Philos. Mag. 91 (32), 4073–4088.

Carslaw, H.S., Jaeger, J.C., 1959. Conduction of Heat in Solids, 2. Clarendon press, Oxford, pp. 8–13.

Caruso, F., Caruso, R.A., Moehwald, H., 1998. Nanoengineering of inorganic and hybrid hollow spheres by colloidal templating. Science 282 (5391), 1111–1114.

Cheng, Y.T., Verbrugge, M.W., 2009. Evolution of stress within a spherical insertion electrode particle under potentiostatic and galvanostatic operation. J. Power Sources 190, 453–460.

Christensen, J., Newman, J., 2006. Stress generation and fracture in lithium insertion materials. J. Solid State Electrochem. 10, 293–319.

DeLuca, C.M., Maute, K., Dunn, M.L., 2011. Effects of electrode particle morphology on stress generation in silicon during lithium insertion. J. Power Sources 196, 9672–9681.

Gao, F., Hong, W., 2016. Phase-field model for the two-phase lithiation of silicon. J. Mech. Phys. Solids 94, 18–32.

Gao, Y.F., Zhou, M., 2011. Strong stress-enhanced diffusion in amorphous lithium alloy nanowire electrodes. J. Appl. Phys. 109, 014310.

Gattinoni, C., Michaelides, A., 2015. Atomistic details of oxide surfaces and surface oxidation: the example of copper and its oxides. Surf. Sci. Rep. 70 (3), 424–444.

Golmon, S., Maute, V., Lee, S.H., Dunn, M.L., 2010. Stress generation in silicon particles during lithium insertion. Appl. Phys. Lett. 97, 033111.

Grantab, R., Shenoy, V.B., 2012. Pressure-gradient dependent diffusion and crack propagation in lithiated silicon nanowires. J. Electrochem. Soc. 159, A584–A591.

Haftbaradaran, H., Gao, H.J., Curtin, W.A., 2010. A surface locking instability for atomic intercalation into a solid electrode. Appl. Phys. Lett. 96, 091909.

Haftbaradaran, H., Song, J., Curtin, W.A., Gao, H.J., 2011. Continuum and atomistic models of strongly coupled diffusion, stress, and solute concentration. J. Power Sources 196, 361–370.

Henkelman, G., Jónsson, H., 2000. Improved tangent estimate in the nudged elastic band method for finding minimum energy paths and saddle points. J. Chem. Phys. 113 (22), 9978–9985.

Henkelman, G., Uberuaga, B.P., Jónsson, H., 2000. A climbing image nudged elastic band method for finding saddle points and minimum energy paths. J. Chem. Phys. 113 (22), 9901–9904.

Huang, C.L., Weng, W.L., Liao, C.N., Tu, K.N., 2018. Suppression of interdiffusion-induced voiding in oxidation of copper nanowires with twin-modified surface. Nat. Commun. 9 (1), 340.

Hui, C., Zr, A., Fy, B., 2020. Mechanical properties of cu nanowires: effects of cross-sectional area and temperature. Mater. Sci. Eng. A 791, 139644.

Iijima, J., Lim, J., Hong, S., Suzuki, S., Mimura, K., Isshiki, A., 2006. Native oxidation of ultra-high purity cu bulk and thin films. Appl. Surf. Sci. 253 (5), 2825–2829.

Kim, S.W., Kim, M., Lee, W.Y., Hyeon, T., 2002. Fabrication of hollow palladium spheres and their successful application to the recyclable heterogeneous catalyst for suzuki coupling reactions. J. Am. Chem. Soc. 124 (26), 7642–7643.

Liu, R., Li, D., Wang, C., Li, N., Li, Q., Lü, X, Spendelow, J.S., Wu, G., 2014. Core-shell structured hollow sno2-polypyrrole nanocomposite anodes with enhanced cyclic performance for lithium-ion batteries. Nano Energy 6, 73–81.

Loeffel, K., Anand, L., 2011. A chemo-thermo-mechanically coupled theory for elastic-viscoplastic deformation, diffusion, and volumetric swelling due to a chemical reaction. Int. J. Plasticity 27 (9), 1409–1431.

Moon, J., Lee, B., Cho, M., Cho, K., 2016. Ab initio and kinetic Monte Carlo study of lithium diffusion in LiSi, Li12Si7, Li13Si5 and Li15Si4. J. Power Sources 328, 558–566.

Oldenburg, S.J., Averitt, R., Westcott, S.L., Halas, N.J., 1998. Nanoengineering of optical resonances. Chem. Phys. Lett. 288 (2-4), 243–247.

Platzman, I., Brener, R., Haick, H., Tannenbaum, R., 2008. Oxidation of polycrystalline copper thin films at ambient conditions. J. Phys. Chem. C 112 (4), 1101.

Plimton, Steve, 1995. Fast parallel algorithms for short-range molecular dynamics. J. Comput. Phys. 117 (1), 1–19.

Prisedsky, V.V., Vinogradov, V.M., 2004. Fragmentation of diffusion zone in high-temperature oxidation of copper. J. Solid State Chem. 177 (11), 4258–4268.

Ryu, I., Choi, J.W., Cui, Y., Nix, W.D., 2011. Size-dependent fracture of Si nanowire battery anodes. J. Mech. Phys. Solids 59, 1717–1730.

Shenoy, V.B., Johari, P., Qi, Y., 2010. Elastic softening of amorphous and crystalline Li–Si phases with increasing Li concentration: a first-principles study. J. Power Sources 195 (19), 6825–6830.

Sondors, R., Kosmaca, J., Kunakova, G., Jasulaneca, L., Ramma, M.M., Meija, R., Kauranens, E., Antsov, M., Erts, D., 2020. Size distribution, mechanical and electrical properties of CuO nanowires grown by modified thermal oxidation methods. Nanomaterials 10 (6), 1051.

Song, J., Wang, L., Zibart, A., Koch, C., 2012. Corrosion protection of electrically conductive surfaces. Metals 2 (4), 450–477.

Su, D., Xie, X., Dou, S., Wang, G., 2014. Cuo single crystal with exposed {001} facets - a highly efficient material for gas sensing and li-ion battery applications. Sci. Rep. 4 (1), 5753.

Tafreshi, S.S., Roldan, A., Leeuw, N., 2015. Hydrazine network on cu(111) surface: a density functional theory approach. Surf. Sci. 637, 140–148.

Tan, E.P.S., Zhu, Y., Yu, T., Dai, L., Sow, C.H., Tan, V.B.C., Lim, C.T., 2007. Crystallinity and surface effects on Young's modulus of CuO nanowires. Appl. Phys. Lett. 90 (16), 163112.

Wei, Y., Bower, A.F., Gao, H., 2010. Analytical model and molecular dynamics simulations of the size dependence of flow stress in amorphous intermetallic nanowires at temperatures near the glass transition. Phys. Rev. B 81 (12), 125402.

Xie, Q., Zhao, Y., Xu, C., Liu, H., Yang, W., 2011. Nanosheet-based titania microspheres with hollow core-shell structure encapsulating horseradish peroxidase for a mediator-free biosensor. Biomaterials 32 (27), 6588–6594.

Yang, H., Fan, F., Liang, W., Guo, X., Zhu, T., Zhang, S., 2014. A chemo-mechanical model of lithiation in silicon. J. Mech. Phys. Solids 70, 349–361.

Zhang, X., Shyy, W., Sastry, A.M., 2007. Numerical simulation of intercalation-induced stress in Li-ion battery electrode particles. J. Electrochem. Soc. 154, A910–A916.

Zhao, K., Pharr, M., Vlassak, J.J., Suo, Z., 2010. Fracture of electrodes in lithium-ion batteries caused by fast charging. J. Appl. Phys. 108 (7), 473.

Zhou, G., Luo, L., Li, L., Ciston, J., Stach, E.A., Yang, J.C., 2012. Step-edge-induced oxide growth during the oxidation of Cu surfaces. Phys. Rev. Lett. 109 (23), 235502.